

Large-Scale, Persistent Nutrient Fronts of the World Ocean: Impacts on Biogeochemistry



Jaime B. Palter, Irina Marinov, Jorge L. Sarmiento, and Nicolas Gruber

Abstract This chapter identifies and describes the large-scale nutrient fronts that span the width of basins and explores the processes that maintain these fronts and those that act against them. In particular, we investigate the nutrient fronts that ring the subtropical gyres and propose that exchange across these fronts represents a critical pathway for nutrients to enter the gyres. However, these biogeochemical fronts most often coincide with dynamical fronts or jets, which are often considered barriers to exchange. Therefore, our view of ocean fronts as nutrient gateways must be reconciled with their tendency to act as barriers to exchange. Ekman transport is one mechanism that allows for nutrient transport across the surface of the fronts and is shown to be a leading term in the subtropical nutrient budgets. Ring formation and mixing beneath the core of jets are other mechanisms that can mediate cross-frontal exchange and have intriguing implications for nutrient budgets and their variability.

Keywords Lateral exchange, Nutrients, Ocean fronts, Productivity

J.B. Palter (✉)

Department of Atmospheric and Oceanic Sciences, McGill University, Montreal, QC, Canada
e-mail: jaime.palter@mcgill.ca

I. Marinov

Department of Earth and Environmental Science, University of Pennsylvania, Philadelphia, PA, USA
e-mail: imarinov@sas.upenn.edu

J.L. Sarmiento

Atmospheric and Oceanic Sciences Program, Princeton University, Princeton, NJ, USA
e-mail: jls@princeton.edu

N. Gruber

Environmental Physics, Institute of Biogeochemistry and Pollutant Dynamics, ETH Zurich, Zurich, Switzerland
e-mail: Nicolas.gruber@env.ethz.ch

Contents

1	Introduction	26
2	A Description of the Ocean's Biogeochemical Fronts	31
2.1	The Edges of Oxygen Minimum Zones	32
2.2	Subtropical-Subpolar Gyre Boundaries	35
2.3	Biogeochemical Fronts of the Southern Ocean	39
3	The Fronts of the ACC and Their Role in Nutrient and Carbon Return Pathways from the Deep Ocean	42
4	A Closer Look at Cross-Frontal Exchange	45
4.1	Fronts as Barriers: Reviewing Results from Kinematic Analysis	45
4.2	Fronts as Regions of Exchange: Ekman Fluxes	47
4.3	Ekman Fluxes in the Context of Other Nutrient Supply and Demand Terms	49
5	Conclusions and Open Questions	55
	References	57

1 Introduction

Ocean fronts separate dynamically distinct regions of the ocean and are characterized by sharp lateral property gradients (Figs. 1 and 2). The sharpness of these fronts arises as an inherent feature of fluid motion in the presence of stratification and rotation, and narrow fronts are common features of the ocean and atmosphere [1, 2]. Most, but not all, ocean fronts of biogeochemically important constituents, such as nutrients and carbon, coincide with density fronts, narrow regions where density surfaces slope towards the ocean's surface. Such spatial coincidence is most simply explained by the action of the biological pump, which strips nutrients and carbon from the low-density surface waters and transports them as organic matter to denser waters at depth. Thus, just as density increases with ocean depth, so too do nutrients and carbon, and where density surfaces rise in depth, the isosurfaces of these biogeochemical properties rise with them. Indeed, it is difficult to visually distinguish between maps of horizontal gradients of density and nutrients on a depth surface (Figs. 1 and 2).

On either side of these sloping density surfaces or isopycnals, different dynamical and biogeochemical regimes create water masses with dissimilar properties. Therefore, a biogeochemical front does not arise solely from sloping isopycnals but also from property gradients on the isopycnals themselves. These isopycnal property gradients generally reflect the boundaries between different water masses with distinct biogeochemical histories. Differences between density fronts and nutrient fronts also arise because density is a dynamical tracer that influences the velocity field. In situations where temperature and salinity changes are density compensating, nutrients and other tracers can have sharp gradients while density remains essentially constant [e.g., 3, 4]. An example of a nutrient front on a nearly constant density surface is found on the $\sigma_\theta = 26.5$ isopycnal (equivalent to a seawater density of $1,026.5 \text{ kg m}^{-3}$), where strong lateral gradients in nitrate and

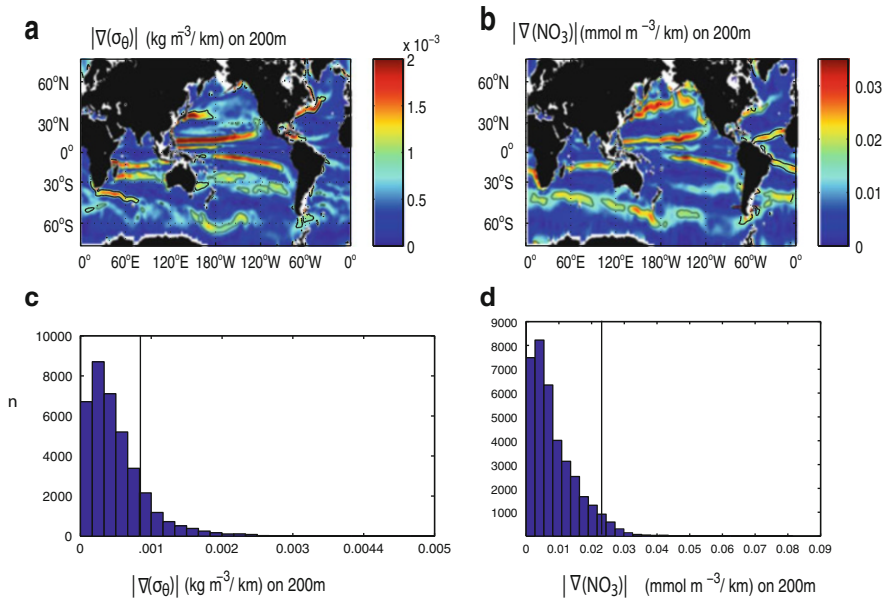


Fig. 1 The lateral gradients of potential density (a) and nitrate (b) at 200 m constructed from World Ocean Atlas 2009 annual means (WOA09 [87], found online at: http://www.nodc.noaa.gov/OC5/WOA09/pr_woa09.html). The contour that corresponds with the 85th percentile of the gradient (i.e., 85% of the gradients are smaller than this contour) is outlined in black. Panels (c) and (d) are histograms of the lateral gradients at 200 m with the 85th percentile shown as a black line. The histograms demonstrate that over most of the ocean the lateral density and nitrate gradients are very small, but their distributions are strongly skewed. The high gradients that form the right tail of the histograms in the lower panels are clearly organized into narrow fronts, as shown in the maps of the *upper panels*

oxygen mark the water mass boundaries that separate the inner tropics from the mid latitudes at 20°S and 20°N (Fig. 3).

Property fronts at the boundaries of water masses are often intensified because steep isopycnal slopes are associated with strong geostrophic jets, which are known to create dynamic barriers to exchange and further isolate the water masses on either side of a front [5–7]. The low- to mid-latitude subtropical gyres are regions where this barrier effect might be particularly important. These regions are laterally homogeneous, well stratified, and bounded by jets that tend to act as barriers to exchange. In the hypothetical extreme case of a subtropical gyre bounded by fronts that inhibit all lateral exchange, property budgets within the gyre would have to balance vertically. This requirement becomes clear when we consider a hypothetical Lagrangian parcel circuiting this gyre, as depicted schematically in Fig. 4. In the absence of lateral exchange across the streamlines that define this gyre, any net downward property flux across the bottom of that parcel’s maximum mixed layer depth must be restored by a corresponding upward flux to maintain steady-state concentrations on timescales longer than a few years [8].

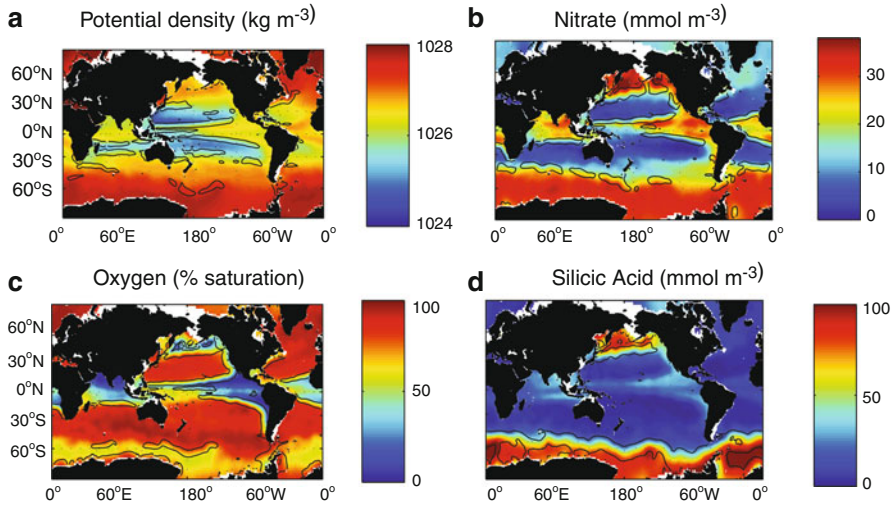


Fig. 2 Properties on 200 m in color with the 85th percentile of their gradients contoured in *black* (i.e., 85% of the gradients are smaller than this contour). (a) Potential density referenced to the surface (kg m^{-3}); (b) nitrate (mmol m^{-3}); (c) oxygen (percent saturation); (d) silicic acid (mmol m^{-3})

Such a requirement for a vertical property balance would be problematic for near-surface biology to maintain its productivity, as biology typically represents a one-way street for nutrients: phytoplankton transform nutrients from the dissolved inorganic form into organic particulate forms, which sink from the illuminated upper ocean constituting the euphotic zone. Sediment trap studies suggest that 10–20% of the organic particles sinking from the base of the euphotic zone continue past a depth of a thousand meters in the tropics and subtropics [9–11], leading to a net loss of these nutrient elements from the subtropical gyre system. Local vertical processes in the stratified, downwelling subtropical gyres cannot restore these lost nutrients. Instead, we suggest a two-step process for returning these nutrients to the euphotic zone of the gyres. First, upwelling and vertical mixing in the regions surrounding the gyre bring the nutrients to shallower depths. Second, advection and mixing across the fronts then resupply these nutrients to the gyre regions where they were originally lost by vertical export. Indeed, cross-frontal exchange of nutrients has been shown to be critically important in fueling primary productivity in low latitudes. In particular, the equatorward Ekman transport of nutrients across the northern subtropical boundaries is an important source of nutrients to the subtropical North Atlantic and North Pacific [8, 12, 13].

It has also been hypothesized that exchange across the Antarctic Circumpolar Current (ACC) plays a critical role in restoring nutrients lost to depths beneath the global pycnocline and maintaining the biological productivity of much of the mid- and low-latitude ocean [14–17]. It is argued that without this Southern Ocean nutrient source, the sum of the vertical processes that transport nutrients upwards across the thermocline everywhere outside the Southern Ocean would be insufficient

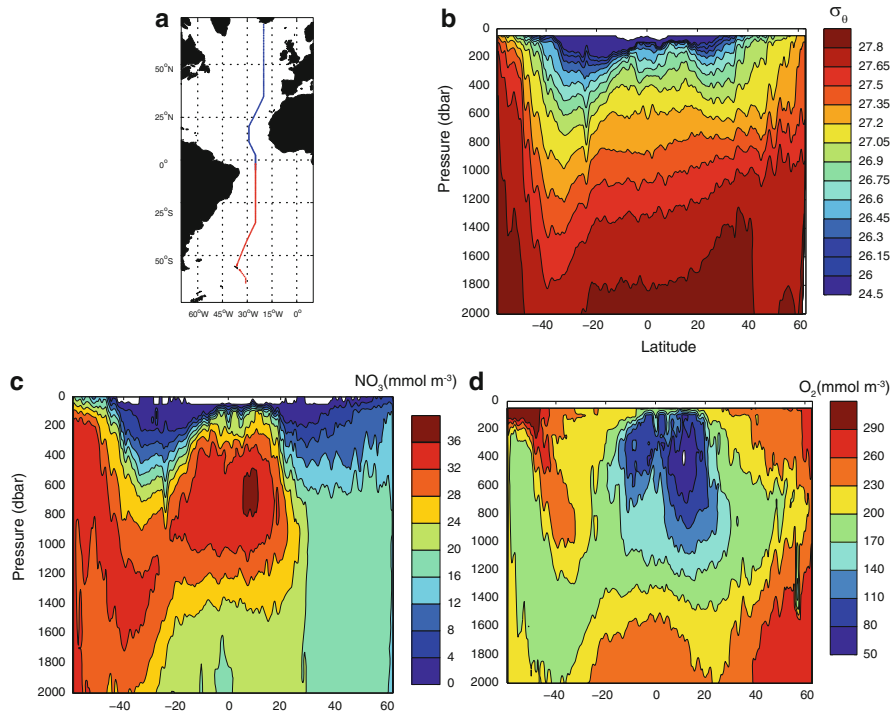


Fig. 3 Meridional section of density nutrients and oxygen through the Atlantic. **(a)** The station locations of WOCE section A16n occupied in June–August 2003 (*blue*) and A16s occupied January–February 2005 (*red*). These stations have been stitched together to plot a continuous section as a function of depth and latitude: **(b)** Potential density anomaly referenced to the surface. **(c)** Nitrate (mmol m^{-3}), **(d)** oxygen (mmol m^{-3}). Nitrate and oxygen fronts generally coincide with density fronts (as is also apparent in Fig. 2). In addition, water mass boundaries give rise to biogeochemical fronts along isopycnals, most apparent near 20°N and 20°S where gradients in nitrate and oxygen are much stronger than in potential density

to restore all of the nutrients that slowly leak across its base. Instead, wind-driven upwelling in the Southern Ocean and the cross-ACC Ekman transport of nutrients is invoked as a restoring mechanism for nutrients to the global thermocline [14]. Therefore, cross-frontal exchange appears to be critical in determining the transport of nutrients back to the near-surface ocean, controlling the productivity of the mid- and low latitudes to a substantial degree.

Here we attempt to reconcile these two views of fronts as the barriers and the gateways to property exchange. By synthesizing a variety of hydrographic data in a dynamical context, we address the questions: Where are the ocean’s most important biogeochemical fronts? What are the dynamical and biogeochemical processes that maintain these fronts? How does exchange across them shape biogeochemical processes in the relatively homogenous ocean gyres bounded by such fronts? In exploring these questions, we first define the ocean’s large-scale biogeochemical

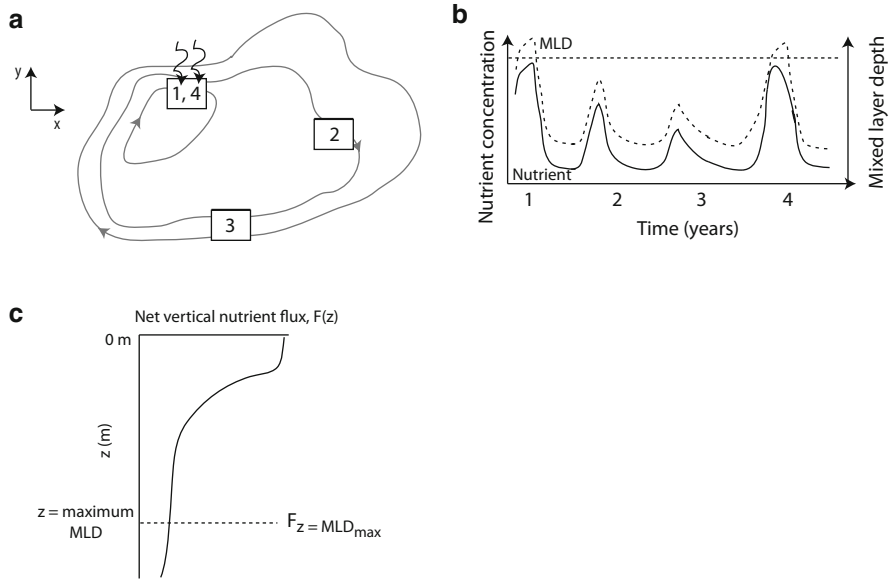


Fig. 4 A schematic for a hypothetical parcel transiting a subtropical gyre in the ocean mixed layer, inspired by Williams and Follows [13]. **(a)** The parcel transits a closed loop in a subtropical gyre in 4 years, with each year labeled in the box representing the parcel. **(b)** It starts in its most poleward position, where mixed layers (*dotted line*) are at a maximum along its trajectory and the seasonal vertical entrainment flux creates high mixed layer nutrient concentrations (*solid line*). In subsequent winters, shoaling of the mixed layer depth along the parcel's trajectory reduces the entrainment flux from below and gives rise to a decline in mixed layer nutrient concentrations. **(c)** There is a net vertical flux of nutrients (i.e., the downward export of nutrients) to depths beneath the maximum mixed layer along the parcel's trajectory. Thus, a lateral supply of nutrients is required to restore nutrient concentrations to their initial concentrations at the parcel's initial position. We propose that a cross-frontal nutrient flux (*curvy arrows* in panel *a*) is a critical supply pathway by which nutrients are restored to the mixed layer

fronts and explore the dynamical and biogeochemical regimes that maintain them. Here, we look primarily at the macronutrient fronts of nitrate, phosphate, and silicic acid. Iron is also an important limiting nutrient, but observations are still too sparse to identify large-scale fronts in iron. Next, we investigate the role of cross-frontal exchange in providing nutrients to the homogenous regions bounded by fronts. Williams and Follows [8] provide an excellent reference for the mechanisms by which cross-frontal exchange helps maintain biological production. Our exploration is therefore focused on identifying the specific locales in the ocean where fronts separate water masses with strongly contrasting biogeochemical signatures and on providing simple diagnostics of their potential impact on biogeochemical processes.

2 A Description of the Ocean's Biogeochemical Fronts

The vast majority of the ocean's volume is characterized by strong vertical stratification and weak lateral property gradients, at least when averaged over several mesoscale eddy time and length scales, i.e., timescales of months and length scales of several hundreds of kilometers. In contrast, fronts have lateral property gradients an order of magnitude greater than their surrounding regions (Fig. 1). Our focus is on the large-scale, persistent, biogeochemical fronts of the open ocean. Before launching our discussion of these fronts, we recognize the important biogeochemical fronts in the coastal ocean that fall beyond the scope of this chapter. These include the fronts that arise at the edges of coastal upwelling regions, where the thermocline and nutricline break the ocean's surface under the influence of an alongshore wind stress [18]. Three additional coastal fronts can be found at the edges of shallow shelf seas: a freshwater front, influenced by the input of fresher estuarine water into the coastal zone; the shelf sea tidal mixing front, caused by the competition between surface buoyancy forcing and tidal mixing; and the shelf-break front, a site of enhanced tidal and wind-driven mixing where the relatively flat continental shelf transitions to the steeper incline of the continental slope [19, 20]. All of the shelf sea fronts divide coastal waters from the open ocean. Because coastal waters are generally more nutrient rich than the offshore waters, the shelf sea fronts often mark stark biogeochemical boundaries. Furthermore, strong mixing at these fronts is thought to provide nutrients to the euphotic zone and enhance productivity.

Our discussion of basin-scale biogeochemical fronts is guided by the maps of density, nutrients, and oxygen at 200 m (Figs. 1 and 2). We examine property gradients at 200 m to focus on persistent fronts that have a near-surface expression: the fronts at the edges of the ocean's oxygen minimum zones, those at the subtropical-subpolar boundaries, and those circumnavigating the globe in the Southern Ocean. It is across these fronts that mixing and advection bring nutrients into the euphotic zone to directly influence primary productivity in the neighboring regions. By looking at 200 m instead of directly at the surface, we avoid dealing with spatial variability driven exclusively by surface processes, such as biological drawdown of nutrients and air-sea heat and freshwater exchange. Shelf-break fronts are typically found at depths shallower than 200 m, so the maps of Figs. 1 and 2 will not capture these features. Vertical sections suggest that there are also biogeochemical fronts deeper in the ocean interior that fall outside the scope of this chapter (e.g., at the boundary separating oxygen-poor AAIW from oxygen-rich Mediterranean waters at approximately 20°N in the Atlantic as seen in Fig. 3d).

In many regions, notable features in satellite-derived chlorophyll concentration are coincident with the nutrient fronts, providing an additional motivation to understand what sets the locations of these fronts. In particular, the transition region between the low-chlorophyll North Atlantic and North Pacific subtropical gyres and their neighboring chlorophyll-rich regions coincide with strong nutrient fronts (Fig. 5). In the open waters of the Indian and Atlantic sectors of the Southern Ocean, the chlorophyll concentration maxima overlap with the nutrient fronts (Fig. 5).

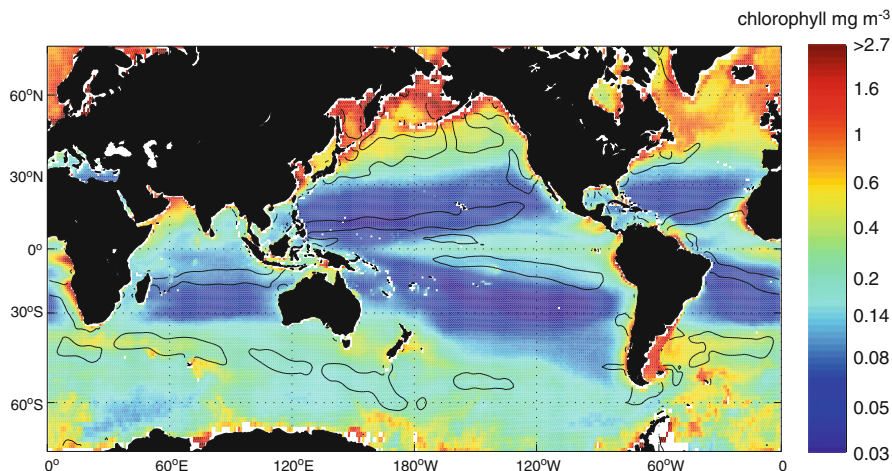


Fig. 5 Satellite-observed chlorophyll from SeaWiFS Level 3 data (*colors*) averaged over the period 1997–2009. Because chlorophyll concentrations in the global ocean are distributed lognormally [111], concentrations are plotted on a log scale. Black contours show the 85th percentile of the nitrate gradient (as in Fig. 2b)

We begin in the next section by describing several of the large-scale, persistent biogeochemical fronts of the global ocean: at the edges of oxygen minimum zones (Sect. 2.1), across western boundary currents of the North Pacific and North Atlantic (Sect. 2.2), and across the ACC (Sect. 2.3). In Sect. 2, we also briefly discuss the balance between the mechanisms that maintain these sharp gradient regions and the processes that transport biogeochemical constituents across them. In Sect. 3, we explore the far-reaching consequences on nutrient and carbon budgets of cross-frontal exchange in the ACC region. Section 4 attempts to reconcile the two views of fronts, as both barriers and gateways to property exchange, and quantifies cross-frontal nutrient supply relative to other supply pathways of nutrients in several ocean regions. Finally, we summarize and conclude in Sect. 5.

2.1 The Edges of Oxygen Minimum Zones

Among the most visually striking biogeochemical fronts are those found at the edges of the ocean’s oxygen minimum zones (OMZs) in the tropical oceans and North Pacific (Figs. 2c and 6). These fronts are produced by the interplay of biology and physics. In the ocean interior, oxygen is consumed by the remineralization of organic matter and it is replenished by the advection and mixing of oxygen into the domain. It is no coincidence that oxygen minimum zones coincide with the ocean’s so-called shadow zones where subsurface streamlines recirculate without a direct connection to the surface ocean. Whereas the subsurface layers of the subtropical gyre are oxygenated by the formation and spreading of mode waters, the shadow zone is found in the space created between the subtropical gyre circulation and the

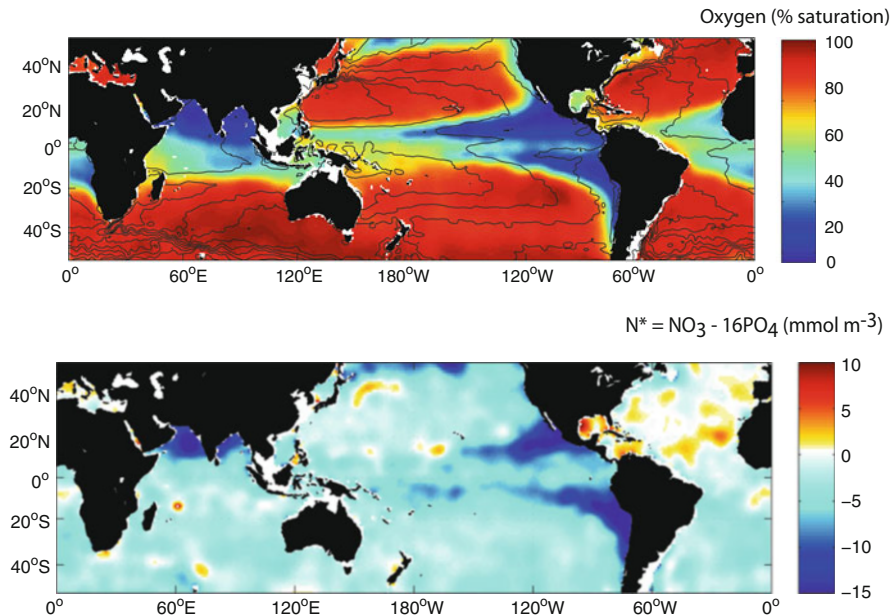


Fig. 6 Oxygen (percent saturation) and N^* (mmol m^{-3}) on 200 m with sea surface height (mean dynamic topography) from the altimetry-based climatology of Rio and Hernandez [23]. Contours of the mean dynamic topography resemble geostrophic streamlines at the ocean's surface

basin's eastern boundary. Here, exchange with the neighboring subtropical gyre is slow and the subsurface layers are shielded from exchange with the overlying atmosphere by a shallow surface mixed layer.

The shadow zone circulation arises from constraints on the potential vorticity (PV) budget, which cause the geostrophic streamlines that close the subtropical circulation to pull away from the basins' eastern boundaries [21, 22]. For flows with low Rossby number (i.e., in flows where the Coriolis term is much larger than the relative vorticity), PV is approximately equal to f/H , where f is the planetary vorticity and H is the thickness of an isopycnal layer. In the nearly inviscid ocean interior, potential vorticity is conserved. Therefore, along the trajectory of a fluid parcel, the quotient f/H remains nearly constant and changes only through slow mixing with surrounding fluids. Applying this PV conservation constraint to a fluid parcel following the eastern equatorward-flowing branch of the subtropical gyre circulation requires that the layer thickness (H) decreases in order to compensate for the decrease in the planetary vorticity (f). However, any meridional change in layer thickness creates a meridional pressure gradient and a corresponding zonal geostrophic flow. To avoid flow into or out of a basin's eastern boundary, the eastern subtropical circulation is deflected westward [22]. We see manifestations of this physical constraint in ocean observations: contours of sea surface height [23] are clearly deflected to the west at the eastern boundary of the subtropical oceans (Fig. 6). This westward deflection shows that the surface geostrophic flow closing

the anticyclonic, subtropical gyre circulation is found at a distance from the basin's eastern boundary. The shadow zone extends eastwards from the edge of the gyre below a shallow, oxygenated surface layer.

Between the westward deflected streamlines and the continents, the residence time in the thermocline is at a maximum for each basin [24–26]. Overlying and adjacent to these shadow zones are highly productive eastern boundary upwelling systems, where the upwelling of nutrients fuels photosynthetic production of organic matter, a fraction of which is exported to the thermocline. Thus, the oxygen minimum zones result from the combined influence of organic matter export and remineralization in the thermocline and a lack of a direct advective connection with the surface ocean. The situation is quite the contrary in the upper layers of the neighboring subtropical gyres. Here well-oxygenated water masses are formed by wintertime convection at the gyres' poleward edges. These water masses, called subtropical mode waters [27], are transferred into the thermocline, efficiently ventilating its upper layers [21, 28]. Furthermore, low-nutrient conditions in the surface of the subtropical gyres support lower rates of organic matter export than in the upwelling regions [29]. The boundary between these dissimilar physical and biogeochemical regimes marks the ocean's strongest oxygen fronts.

The edges of the oxygen minimum zones are also locales of strong fronts in nitrate and phosphate (Fig. 1 and 2). A basic explanation for these nutrient fronts relies on the same processes as the oxygen fronts. In the subsurface shadow zones, the remineralization of organic matter produces large pools of inorganic nutrients whose principal sink is realized through mixing with lower-nutrient waters in the neighboring gyre [30, 31]. Whereas nutrients in the subtropical gyre are kept low via exchange with the productive surface layer in mode water formation regions [32], their accumulation in the OMZ reflects the lack of physical connection between the subsurface shadow zone and the productive surface layer. In the OMZs of the eastern tropical Pacific Ocean and the northernmost Indian Ocean, there is a sink for nitrate: the microbial respiration of nitrate and/or ammonium to gaseous nitrogen, a process known as denitrification. Because denitrification is slightly less energetically favorable than aerobic respiration, it occurs in the eastern tropical Pacific Ocean and the northern tropical Indian Ocean where dissolved oxygen concentrations fall below $10 \mu\text{mol kg}^{-1}$, but not in the eastern tropical Atlantic Ocean where the minimum oxygen concentrations typically exceed $30 \mu\text{mol kg}^{-1}$ [33, 34].

Whereas nitrate (NO_3^-) and phosphate (PO_4^{3-}) are typically utilized and remineralized in a ratio that averages 16:1, denitrification removes only nitrate, leaving phosphate concentrations unchanged. Thus, a useful tracer that reflects the occurrence of denitrification is $\text{N}^* = \text{NO}_3^- - 16\text{PO}_4^{3-}$ [35]. The depressed N^* at 200 m in the OMZs reflects the denitrification that occurs in ocean's lowest oxygen waters (Fig. 6b). At the edges of the OMZ, an N^* front reflects the boundary between the nitrate-depleted water from the center of the OMZs with the relatively NO_3^- -rich neighboring regions. Leakage of low- N^* water from the Pacific and Indian OMZs clearly influences the mid-depths of the basins far beyond the edges

of the ocean's shadow zones. In the North Atlantic a front divides the N^* maximum waters of the subtropical gyre from the tropical regions. This front is thought to divide the salty subtropical waters where N^* is added via nitrogen fixation from the fresher tropical waters in the North Equatorial Current [35], which are influenced by the low- N^* waters formed in the Southern Ocean [36, 37].

2.2 *Subtropical-Subpolar Gyre Boundaries*

Several aspects of the ocean's subpolar gyre circulation maintain high nutrient concentrations near the surface. First, wind-induced upwelling provides a flux of nutrients from intermediate depths in the ocean to the surface [38]. Second, nutrients flowing poleward in the stratified western boundary currents are advected into the subpolar seasonal boundary layer, a process called induction [37]. Finally, deep wintertime mixing mines these nutrients from the subsurface, returning seasonally lost nutrients to the euphotic zone [38]. This relatively high availability of nutrients together with deep surface mixed layers tend to create an environment where light, rather than nutrients, limits photosynthesis throughout much of the year [e.g., 39, 40]. In stark contrast, the subtropical gyres are downwelling domains with shallower convective mixing. Furthermore, in the Northern Hemisphere subtropical gyres, nutrients are consumed at the gyre's northern flank at the time of mode water formation. This water mass is then subducted with a low-nutrient signature, further endowing the subtropics with a nutrient-depleted upper thermocline [e.g., 32, 37]. Given these dynamical differences, it is unsurprising that the subtropical-subpolar boundaries constitute strong biogeochemical frontal regions (recall Fig. 2). In both the North Atlantic and North Pacific surface and thermocline waters, this boundary marks a transition from low nitrate concentrations in the subtropics to high concentrations in the subpolar gyres and a related transition from low to high chlorophyll in the surface ocean (Fig. 5).

2.2.1 **The Kuroshio**

The Kuroshio jet marks the transition between the nutrient-depleted surface waters of the subtropical North Pacific and the nutrient-rich surface waters of the region north of the current (Fig. 7). In addition to being a strong nitrate and phosphate front, the Kuroshio is also the only front north of the ACC where high silicic acid concentrations outcrop. Outside of the subpolar North Pacific and the ACC, the global thermocline is severely silicic acid-depleted, a feature that has long fascinated oceanographers [41]. Recent work suggests that subduction on the equatorward edge of the ACC floods the lower thermocline with water that is depleted in silicic acid, setting this property in the global thermocline [14, 15], a concept we will return to in Sect. 3. Only in the ACC and in the subpolar North Pacific and its marginal seas do mixing and upwelling return deep silicic acid to the upper thermocline and surface ocean. The sharp surface gradients prompt the questions: Is there an important cross-Kuroshio

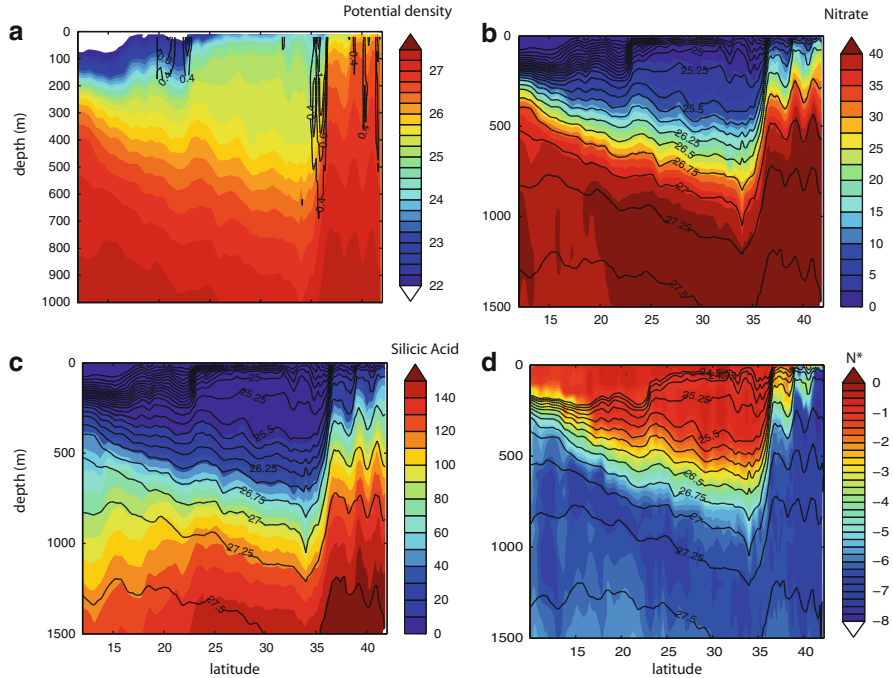


Fig. 7 WOCE section P10 occupied in 2005 from New Guinea to Japan crosses the Kuroshio and the North Pacific subtropical mode water region. (a) Potential density referenced to the sea surface (color) with velocity (contours in m s^{-1}) measured by a shipboard ADCP. (b) Nitrate (mmol m^{-3}). (c) Silicic acid (mmol m^{-3}). (d) N^* (mmol m^{-3}). The Kuroshio appears as a strong jet at approximately 35°N and clearly divides the domain between the relatively nitrate and silicic acid poor subtropical gyre and a nutrient rich region north of the Kuroshio. The thermocline shows strong nitrate depletion relative to phosphate (negative N^*), a signal that rises to the surface in the Kuroshio

exchange of nitrate and silicic acid? What are the physical processes that facilitate such exchange?

The importance of cross-Kuroshio transport has recently been highlighted by several studies [12, 42, 43]. Ayers and Lozier [12] showed that seasonal variability in the position of the North Pacific chlorophyll front was tied to the Ekman advection of nutrients across the Kuroshio. Qiu and coauthors [42, 43] suggest that variability in eddy-mediated cross-Kuroshio exchange is reflected in the temporal variability of the Subtropical Mode Water (STMW). The STMW is a pool of weakly stratified water between the $\sigma_\theta = 25.25$ and 25.5 isopycnals that is formed by convection each winter at the poleward edge of the subtropical gyre [27] and extends from the equatorward edge of the Kuroshio to the southern limit of the subtropical gyre. The temperature, salinity and thickness of the STMW appear to be strongly influenced by the number of rings formed by the Kuroshio [42, 43]. These rings are thought to be one of the principal mechanisms for exchanging fluid across jets [44].

Similar to what has been shown in the subtropical North Atlantic [32], the North Pacific STMW appears to inject a wedge of relatively nutrient-poor water above the nutricline (Fig. 7b, c). The nutrient concentrations in the mode water are set by a competition between biological drawdown on one hand and the supply of nutrients via vertical entrainment from the underlying nutricline and cross-frontal nutrient transport on the other. Given that the stratified waters crossing from the region north of the Kuroshio into the subtropics are high in nitrate and silicic acid and low in N^* (Fig. 7) and that these rings are thought to set the physical properties of the North Pacific STMW [42, 43], we speculate that the rings shed by the Kuroshio may exert an important influence on the temporal variability of nutrient concentrations and ratios in the STMW. The Kuroshio has two dynamic states, one with a relatively stable path and the other with a highly variable path and vigorous ring formation [42]. Therefore, we hypothesize that variability in the nutrient composition of the gyre may be linked to the dynamic state of the Kuroshio, the number of rings shed from the current, and the Ekman flux across it. Because the STMW comprises the nutrient reservoir at the base of the euphotic zone for much of the western subtropical gyre, such variability could possibly exert a critical control on primary productivity and perhaps species composition in the gyre.

2.2.2 The Gulf Stream

Similar to the Kuroshio, the Gulf Stream forms the boundary between the nutrient-rich subpolar North Atlantic and the depleted waters of the subtropics (Fig. 8). However, a comparison of silicic acid concentrations in the North Atlantic (Fig. 8c) with those of the North Pacific (Fig. 7c) reveals that the Gulf Stream region has roughly 15% the silicic acid found in the Kuroshio region. The low Gulf Stream silicic acid concentrations are consistent with the view that silicic acid-depleted water is advected in the shallow limb of the Meridional Overturning Circulation (MOC) [14], as the Gulf Stream is a principal pathway by which the shallow MOC enters the North Atlantic. The low-silicic acid signature of the Southern Ocean water masses is discussed in detail in Sect. 2.3 on Southern Ocean Fronts.

A number of observational and modeling studies have confirmed that the Gulf Stream is a conduit of nutrients imported from outside the North Atlantic [36, 37, 45–47]. These imported nutrients in the Gulf Stream are suggested by the cross-stream nutrient distributions when plotted as a function of density (Fig. 8d), which show elevated nutrient concentrations that coincide with the high-velocity core in the Gulf Stream. The temperature and salinity signature of the Gulf Stream's high-nutrient waters has been used to link these nutrients to water masses imported in the shallow limb of the MOC [45]. Along the length of the Western Boundary Current, the elevated nutrient concentrations generally decline, especially for the densest isopycnals [45]. This along-stream decline in nutrient concentrations suggests that the Gulf Stream is a source of nutrients to the northern recirculation gyre and/or the subtropical gyre via isopycnal mixing. Thus, the exchange of waters between the Gulf Stream and its neighboring regions brings nutrients from distant locales to

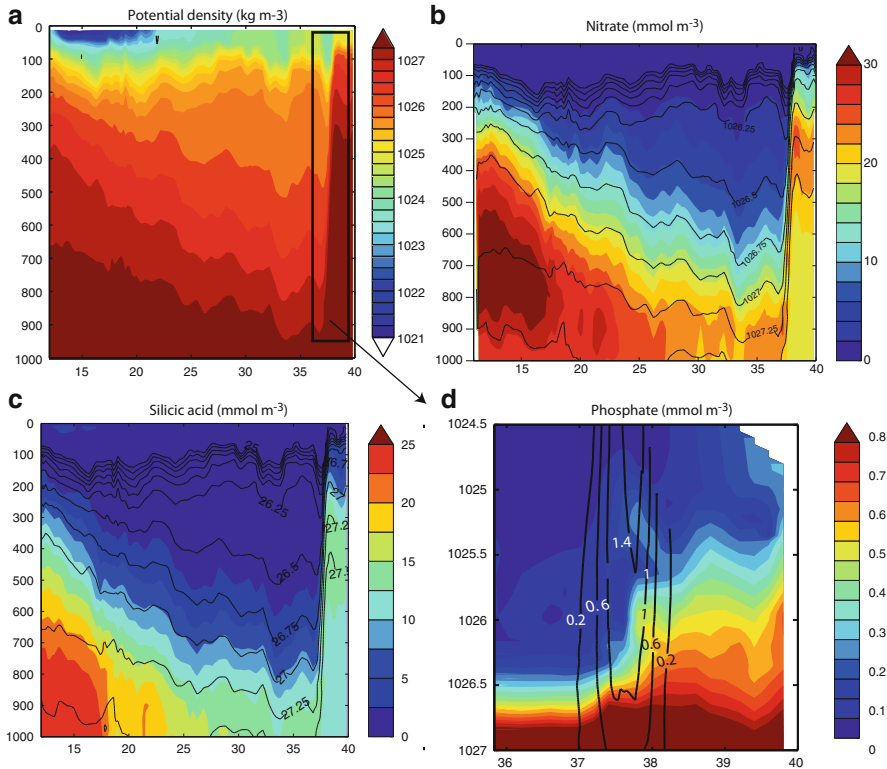


Fig. 8 WOCE Section A22 occupied in 2003 through the Gulf Stream along 64°W . (a) Potential density referenced to the sea surface (*color*). (b) Nitrate (mmol m^{-3}). (c) Silicic acid (mmol m^{-3}). (d) Phosphate (mmol m^{-3}) in color and velocity (m/s) in black contours as a function of density and latitude in a narrow region encompassing the Gulf Stream (outlined in panel a). The high-velocity core of the Gulf Stream corresponds with a bullet of elevated phosphate that can be traced to waters imported in the shallow limb of the MOC [112]

the subtropical gyre. Two important consequences of such exchange are that phosphate advected northward in the shallow MOC may help sustain North Atlantic primary productivity [14, 37] and biological nitrogen fixation [36].

While the recent work by Qiu and coauthors [42, 43] suggests a critical role for Kuroshio rings in setting the PV of the North Pacific STMW, rings shed from the Gulf Stream are thought to be a relatively minor player in tracer exchange in the Atlantic. Bower et al. [5] evaluated the role of ring formation in the subtropical oxygen budget with a scale analysis that used typical properties of Gulf Stream rings and the frequency of their formation. The Kuroshio studies combined satellite and in situ data to study the influence of particular rings on the PV budget of the North Pacific subtropical mode water [42, 43]. The question remains whether the difference in the importance of rings for the North Atlantic and North Pacific is due to differences in the tracers studied (i.e. PV or oxygen),

differences in the dynamics of exchange across the gyres' western boundary currents, or a difference primarily in the techniques used to study the rings. In any case, variability in the Gulf Stream is not known to manifest as variability in ring formation as it does in the Kuroshio. Thus, North Atlantic subtropical gyre nutrient variability may be governed by a distinct set of processes, with possibilities including wind-driven Ekman exchange, eddy exchange that does not result in ring formation, and/or variability in the quantity of nutrients imported in the shallow limb of the MOC and recirculated in the subtropical gyre.

2.3 Biogeochemical Fronts of the Southern Ocean

More than any other region, the Southern Ocean has been defined by its many fronts [e.g., 48–50]. Sharp meridional gradients in temperature and salinity have long been used to divide the Southern Ocean into distinct dynamical provinces. In this section we focus on the Southern Ocean Fronts within the ACC, where more than 100 Sv ($1 \text{ Sv} = 10^6 \text{ m}^3 \text{ s}^{-1}$) of eastward transport circumnavigates the globe [50]. The current is organized into a series of narrow jets, which have been historically grouped into three circumpolar fronts. These fronts, listed from south to north, are the Southern ACC Front (SACCF), the Antarctic Polar Front (APF), and the Subantarctic Front (SAF). In addition to the fronts in the ACC, a Subtropical Frontal Zone (STFZ) bounded by fronts to the north and south can be found north of the ACC (Fig. 9). Traditionally, hydrographic properties and water mass features have been used to define only three ACC fronts, but recent research has revealed that they can split into more than 9 narrower jets or frontal filaments [51], each associated with strong lateral property gradients, swift currents, and the rapid shoaling of subsurface water masses. These fronts are not necessarily continuous, as they can merge and split and are temporally variable [51–53]. Chlorophyll concentrations follow these streamlines even at the scale of mesoscale eddies, a dependence traced in part to the upwelling of nutrients at many of the fronts [54]. Grouping these narrow, discontinuous jets into three ACC fronts remains a useful organizing framework to understand the outcropping of nutrient properties and the cross-front exchange of these nutrients.

Many of the biogeochemical fronts in the Southern Ocean can be linked to the presence of various water masses with distinct properties. As a consequence of wind-driven upwelling and mixing, dense Circumpolar Deep Water (CDW) rises in depth south of the APF (Fig. 10). The most voluminous water mass found in the ACC, CDW is divided into Upper Circumpolar Deep Water (UCDW) and Lower Circumpolar Deep Water (LCDW) based on a variety of contrasting properties. The LCDW is characterized by a salinity maximum ($S > 34.73$) and a subsurface nutrient minimum, both of which can be traced to its origins as North Atlantic Deep Water [55]. In contrast, the UCDW is characterized by an oxygen minimum and nutrient maximum, reflecting deep waters being returned from the lower latitudes of the Indian and Pacific Ocean [56]. Antarctic Intermediate Water (AAIW), characterized by a salinity minimum, is found above the UCDW. The vertical property gradients caused by the stacking of UCDW, LCDW, and AAIW become horizontal gradients

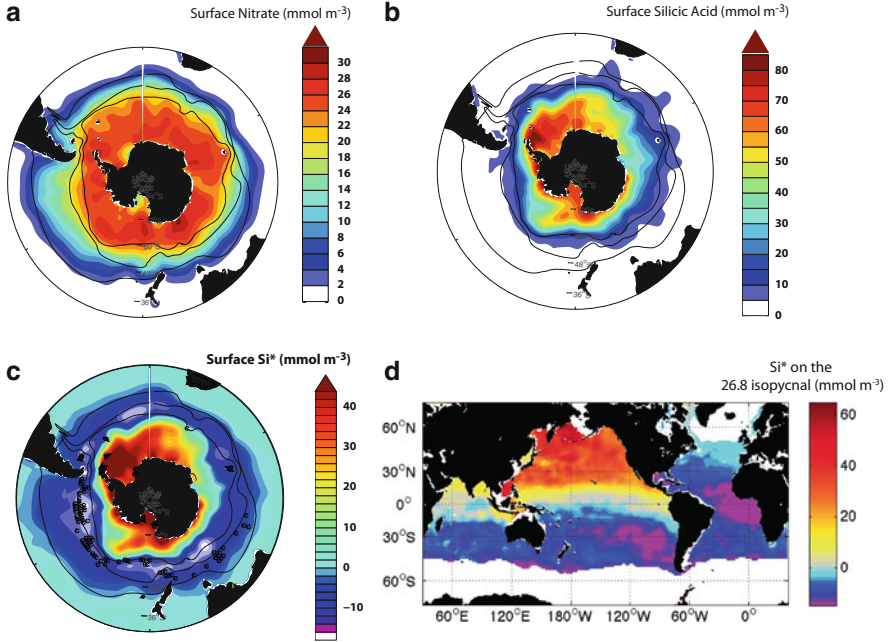


Fig. 9 Polar stereographic maps of the Southern Ocean (South Pole to 30°N) surface nutrient concentrations and the global spreading of its low Si^* signal on the $\sigma_{\theta} = 26.8$ isopycnal, after Sarmiento et al 2004. (a) Surface nitrate (mmol m^{-3}). (b) Surface silicate (mmol m^{-3}). (c) Surface $\text{Si}^* = \text{silicate} - \text{nitrate}$ (mmol m^{-3}) in color. The black dots mark the locations of winter maximum mixed layer depth greater than 400 m, from the climatology of de Boyer Montégut et al. [82]. (d) Si^* on the $\sigma_{\theta} = 26.8$ isopycnal, where nutrient concentrations were interpolated from pressure surfaces to the isopycnal. In the Polar Stereographic maps, the *black contours* show the position of the major circumpolar fronts of the Southern Ocean defined according to Belkin and Gordon [48]. From south to north they are the Antarctic Polar Front (APF), the Subantarctic Front (SAF), and the Southern Subtropical Front (STF). The nutrient data in panels a–c are taken from WOA09 [87]. Panel d is reproduced from Palter et al. [76]

by the action of upwelling in the ACC; to first order, the tilting of these vertical gradients is what produces the biogeochemical fronts across the southern ACC. Next, we briefly introduce the properties of the three traditional ACC fronts from south to north. The goal of this terse introduction is to provide a context for the discussion of nutrient and carbon return pathways from the deep ocean (Sect. 3); the interested reader is directed to Artamonova and Belkin (this volume) for a more thorough discussion of the chemical fronts of the Southern Ocean.

2.3.1 The Southern ACC Front (SACCF)

The Southern ACC Front (SACCF) is marked by large meridional temperature gradients associated with the southward shoaling of the UCDW [50]. The UCDW oxygen minimum and nutrient maximum reside on the $\sigma_{\theta} = 27.6$ isopycnal, which

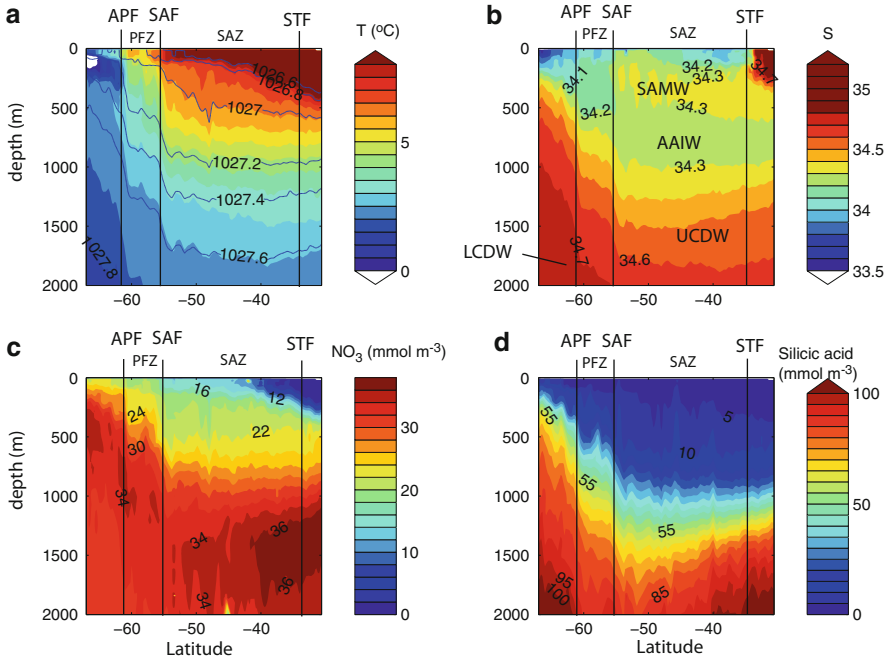


Fig. 10 The P18 WOCE section along 103°W in the Pacific Sector of the Southern Ocean. Properties are a) potential temperature (*colors*) and potential density (contours), (b) salinity, (c) nitrate, and (d) silicic acid. The approximate locations of the Antarctic Polar Front (APF), Subantarctic Front (SAF), and Subtropical Front (STF) are marked by vertical lines, according to the water mass property definitions of Orsi et al. [50] and Belkin and Gordon [48], as synthesized in Pollard et al. [55]. The Subantarctic Zone (SAZ) lies between the SAF and STF; the Polar Frontal Zone (PFZ) lies between the PF and SAF; both are labeled above panel a. The Southern ACC Front (SACCF) is very near the southern edge of this section. Water masses are labeled in panel b: Subantarctic Mode Water (SAMW), Antarctic Intermediate Water (AAIW), Upper Circumpolar Deep Water (UCDW), and Lower Circumpolar Deep Water (LCDW)

rises to 500 m at the SACCF. In contrast, the denser and silicic acid-rich LCDW penetrates south of the SACCF and beyond the southern boundary of the ACC, the southernmost circumpolar contour of the ACC found in Drake Passage. The LCDW reaches the Antarctic continental shelves where it mixes with shelf waters to form dense Antarctic Bottom Water (AABW) that sinks downslope and spreads northward. There is also a shelf-break front surrounding the Antarctic Continent called the Antarctic Slope Front, which has been shown to play a critical role in the formation of AABW [56, 57].

2.3.2 The Antarctic Polar Front (APF)

The Antarctic Polar Front (APF) marks a change in the balance of stratification, from salinity-dominated stratification everywhere south of the APF to approximately

equal contributions to stratification by temperature and salinity north of the APF [55]. The APF is also the northernmost extension of the temperature minimum waters (approximately 2°C), a remnant of winter convection commonly called the Antarctic Winter Water after Mosby [58]. Thus, the zone between the APF and the SACCF is characterized by the presence of the upwelling UCDW, along with its signature oxygen minimum and nitrate maximum. The APF also represents the Southern Ocean silicic acid front, separating silicic acid-rich waters in the upwelling Antarctic Zone from silicic acid-poor waters in the Subantarctic Zone (Figs. 9 and 10).

2.3.3 The Subantarctic Front (SAF)

The Subantarctic Front (SAF) is the northernmost frontal jet that passes through Drake Passage. Like the APF, the SAF also marks a change in the balance of stratification, this time from the Antarctic Polar Frontal Zone where temperature and salinity contribute equally to stratification to a temperature-dominated Subantarctic Zone north of the SAF [55]. The SAF is identified by the northward subduction of the salinity minimum (salinity less than 34) associated with the well-oxygenated AAIW. South of the SAF in the Polar Frontal Zone, the lowest salinity water is found at the surface; this minimum descends at the SAF to depths greater than 400 m [50]. North of the SAF, nitrate-rich, silicic acid-depleted Subantarctic Mode Water is subducted from the surface to the thermocline [14].

2.3.4 The Subtropical Frontal Zone (STFZ)

The Southern Ocean's natural equatorward boundary is the Subtropical Frontal Zone, a 400–500 km wide region bounded by two sharp fronts: the North and South Subtropical Fronts [48]. These fronts separate the relatively saline subtropical gyre waters (surface salinities greater than 35.5 g kg⁻¹) from the fresher subantarctic waters and are often coincident with strong gradients at the ocean's surface in chlorophyll [59].

3 The Fronts of the ACC and Their Role in Nutrient and Carbon Return Pathways from the Deep Ocean

In the introduction, we proposed a two-step process for returning nutrients to the euphotic zone: (1) upwelling and vertical mixing in the regions surrounding the gyre bring the nutrients to shallower depths and (2) advection and mixing across the frontal region then redistribute these nutrients back into the gyres. The frontal regions of the Southern Ocean are thought to be pivotal to the first step of this process, providing a locale where nutrients return from abyssal waters to the pycnocline [14, 17, 60]. As a consequence of its long residence time in the ocean interior, the UCDW is rich in nutrients. The upwelling and mixing of this water mass to the surface ocean in the Antarctic Zone south of the APF create the high surface concentrations of nitrate and

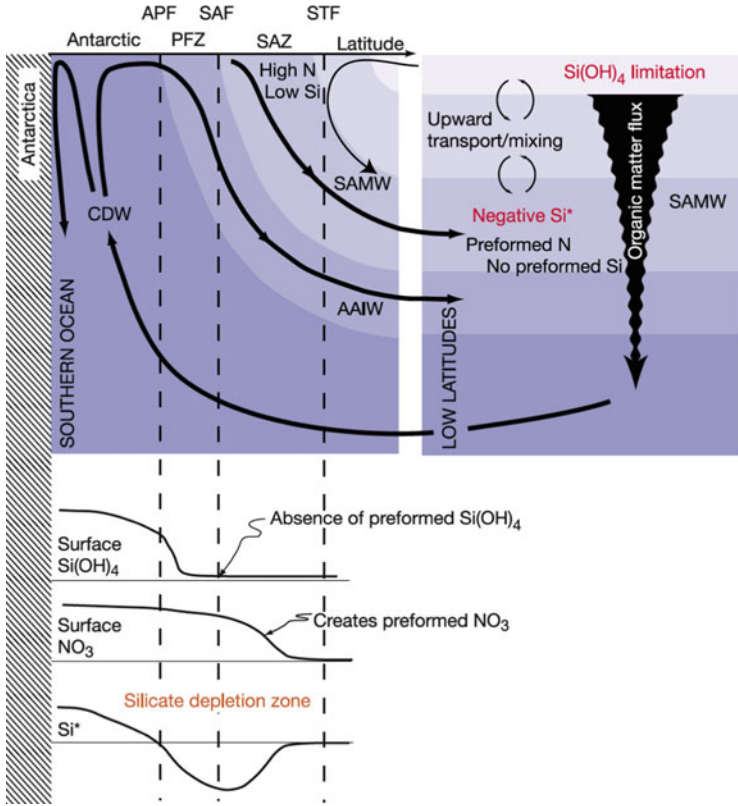


Fig. 11 Southern Ocean control on thermocline nutrient concentrations. Conceptual diagram depicting the Southern Ocean physical and biological processes that form low-Si* waters and feed them into the global thermocline. *Top*, water pathways; *bottom*, details of surface processes. Upper Circumpolar Deep Water (UCDW) upwells to the surface in the Southern Ocean and is transported to the north across the Antarctic Polar Front (APF) into the Polar Frontal Zone (PFZ), where Antarctic Intermediate Water (AAIW) forms, and then across the Subantarctic Front (SAF) into the Subantarctic Zone (SAZ), which is bounded to the north by the Subtropical Front (STF). Silicic acid is stripped out preferentially over nitrate as the water moves to the north, thus generating negative Si* values. This negative-Si* water is a signature of Subantarctic Mode Water (SAMW), which sinks into the base of the main thermocline and feeds biological production in the low latitudes. Lightly modified from Sarmiento et al. [14] to reflect that a portion of the SAMW source water is supplied from the subtropics as in Iudicone [113] and Talley [114]

silicic acid apparent in the surface maps (Fig. 9) and the meridional section in the Southern Ocean’s Pacific Sector (Fig. 10). A portion of the upwelled UCDW is advected northward with the Ekman transport into the Polar Frontal Zone and Subantarctic Zone, as depicted schematically in Fig. 11. There, it is mixed with subtropical waters and subducted as an important constituent of Subantarctic Mode Water (SAMW).

As the upwelled UCDW moves northward across the APF, phytoplankton consume its various nutrients. Diatoms, the dominant phytoplankton group in the biome, take up

silicic acid and nitrate in a 1:1 ratio under adequate light and nutrient conditions. However, under the stress of scarce iron or light, diatoms preferentially remove silicic acid over nitrate from the water column [61]. Because of severe iron and light limitation of photosynthesis in the Southern Ocean [62, 63], silicic acid is stripped from the northward moving surface waters in the Polar Frontal Zone north of the APF, while elevated nitrate concentrations persist well to the north of the APF. This signature of low silicic acid and high nitrate concentrations at the ocean's surface is found exclusively in the Polar Frontal Zone and Subantarctic Zone [14]. Thus, a useful tracer of the water masses that are formed in this region is their low value of $Si^* = Si(OH)_4 - NO_3^-$ [14]. A band of negative Si^* coincides with the deep mixed layers where SAMW is formed (Figs. 9c and 11). Sarmiento et al. [14] argue that the subsurface pool of negative Si^* is an indication of the spreading of Subantarctic Mode Water (SAMW) by advective and diffusive transport processes. The strength of this argument depends on Si^* being a conserved property; nonconservation of the tracer can arise from differences in remineralization length scales of nitrate and silicic acid, with this effect shown to be of the order of 5 mmol m^{-3} at the depth of the SAMW layer [14]. Because of its high nitrate and low silicic acid concentrations, it is believed that the spreading of SAMW in the thermocline helps sustain low-latitude primary productivity but restricts the abundance of diatoms (Fig. 11) [14]. Related to these ideas, it has further been hypothesized that a change in iron input to the Southern Ocean on glacial-interglacial timescales might have led to changes in the relative leakage of nitrate and silicic acid to the low-latitude pycnocline, causing floral shifts in the Equatorial Pacific and changes in the export of organic matter to the deep ocean [64–66].

Model studies also support the idea that advection across the ACC and subduction of nutrients in the SAMW layer provide a major supply of nutrients supporting low-latitude productivity. Depending on model winds and parameterizations of subgridscale processes, the nutrients returned to the pycnocline in the Southern Ocean frontal regions sustain 33–75% of the productivity at low latitudes [14, 17]. The Southern Ocean control on low-latitude productivity can be traced even more specifically to the region immediately north of the APF. Marinov et al. [60] divided the Southern Ocean into Antarctic and Subantarctic regions roughly equivalent to the zones south and north of the APF and forced modeled surface nutrients to zero in these individual regions. As expected, the removal of nutrients north of the APF in the SAMW and AAIW formation region sharply reduced low-latitude productivity relative to the control model. In vivid contrast, the drawdown of nutrients poleward of the APF had almost no influence on low-latitude productivity.

While these model experiments suggest that the region poleward of the APF is of little consequence for low-latitude productivity, it appears to be critical in setting the ocean-atmosphere carbon balance [60]. In this region, the upwelling of LCDW brings nutrients to the surface ocean where they are inefficiently drawn down by biology. Thus, the newly formed AABW returns to the deep ocean interior with a large load of *performed* nutrients. Performed nutrients are those inorganic nutrients that enter the ocean interior without having fueled primary productivity at the

surface. In the ocean interior, the total nutrient concentration is the sum of preformed and remineralized nutrient concentrations. Remineralized nutrients are added to the inorganic nutrient pool of the ocean interior by the remineralization of organic matter. Preformed nutrients are the signature of inefficiency in the biological pump. A more efficient biological pump utilizes a greater portion of the surface preformed nutrients, converts them to organic material, and increases the remineralized nutrient and carbon concentration deeper in the water column. Therefore, a lower global preformed nutrient inventory signifies a higher remineralized nutrient inventory, greater ocean biological carbon storage, and lower atmospheric carbon dioxide [66–69]. Preformed surface nutrients increase with southward distance across the ACC and are highest south of the Polar Front (Fig. 9) where biological uptake is least efficient. In the model simulations, the intensified drawdown of nutrients in the AABW formation region south of the Antarctic PF reduced the ocean’s preformed nutrient inventory and removed a significant quantity of carbon dioxide from the atmosphere. On the other hand, drawing down nutrients in the intermediate and mode water formation regions north of the PF had far less impact on atmospheric CO₂ on a timescale of a few thousand years, as these preformed nutrients are already efficiently utilized and converted to remineralized nutrients downstream of the water mass formation region on decadal timescales [17]. The conclusion drawn from these model experiments is that on the long ocean equilibrium timescales (thousands of years), the air-sea balance of carbon dioxide is strongly influenced by the quantity of preformed nutrients that sink on the poleward side of the Antarctic Polar Front, while global biological productivity is highly sensitive to the rate at which nutrients are subducted on the equatorward side of the Subantarctic Front (Fig. 10).

4 A Closer Look at Cross-Frontal Exchange

So far, we have identified several of the ocean’s strongest biogeochemical fronts, namely, those at the edges of the subtropical oceans that comprise the majority of the ocean’s surface and in the ACC. We have qualitatively described the importance of exchange across these fronts in returning nutrients from the deep ocean to the pycnocline in the Southern Ocean and from the thermocline to the euphotic zone across the subtropical-subpolar boundaries. Now, we take a closer look at mechanisms of exchange and return to the question of how fronts may serve as both barriers to exchange and gateways for the transport of biogeochemical properties.

4.1 *Fronts as Barriers: Reviewing Results from Kinematic Analysis*

A kinematic framework for studying exchange across jets, introduced by Bower [6] and recently synthesized by Wiggins [44], has proven to be a powerful tool in this line

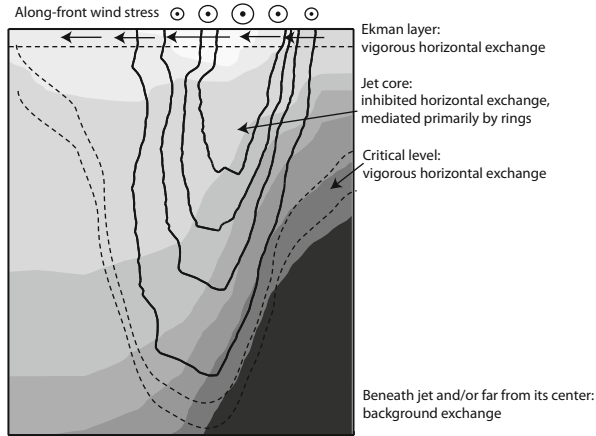


Fig. 12 Schematic of exchange across a front. The *solid lines* are isotachs of positive velocity (flow out of the page) and show the core of the jet; grayscale contours represent density, with higher densities in darker colors. The horizontal dotted line at the top represents the base of the Ekman layer. The *dotted curves* outline the schematized critical level which descends from the near-surface at the front's outer edges to depths beneath the jet's core. An along-front wind stress drives a cross-front Ekman transport. Exchange across the jet is enhanced beneath the jet core at the depth of the critical level and in the Ekman layer, but is inhibited in the jet's core between the Ekman depth and critical level. The limited exchange that is permitted across the center of these jets is mediated primarily by rings shed from the jet [44], with important consequences discussed with regard to North Pacific STMW formation (see Sect. 2.2)

of inquiry and a source of our understanding of ocean jets as barriers to exchange. In the kinematic approach, a flow field is defined from either a model or observations and the trajectories of Lagrangian parcels diagnosed by integrating their position in the flow. Several of these studies have usefully defined the flow as a straight jet perturbed by propagating waves, which force fluid parcels to cross jet streamlines. Such an approach has revealed that cross-frontal exchange is strongly inhibited across the core of jets [6, 70, 71], a view confirmed by the trajectories of floats deployed in the Gulf Stream [72]. On the other hand, lateral exchange is favored where the speed of the jet and the propagation speed of its meanders are approximately equal, locations called steering lines or critical levels. At these critical levels, the motion of a fluid parcel originally in the jet can deviate substantially from the streamlines at the jet's center, permitting exchange between the jet and its surroundings [6, 7, 73].

Near the surface of the ocean, the translation speed at the center of a jet is typically much faster than the propagation speed of its meanders. In contrast, a jet's translation speed and its meander speed are approximately equal at the jet's edges and at depths below the jet's maximum velocity. Thus, there is a three-dimensional surface where turbulent exchange is favored; in a two-dimensional cross section, this surface is defined as a steering line which typically descends from the jet's edges at the surface to depths beneath jet's core (Fig. 12). In the Gulf Stream where swift velocities persist to a depth of 700 m (shown previously in Fig. 7) cross-frontal transport by mesoscale motions is

inhibited between the base of the Ekman layer and the $\sigma_\theta = 27.1$ isopycnal [6]. A similar structure is expected for the Kuroshio. Recent results from an eddy-resolving GCM of the Southern Ocean agree with the results of the kinematic studies: contours of high effective diffusivities driven by eddies follow steering lines as they descend from the northern edge of the ACC to a maximum at 1,500 m beneath the ACC's center [73]. Because the strength of mixing influences the strength of tracer transport, this gradient in horizontal diffusion can produce a tracer flux divergence, a fundamental physical process that is currently unresolved and unparameterized in the coarse-resolution models typically used to simulate climate and biogeochemical cycles. Therefore, how a cross-frontal diffusivity gradient might impact the exchange of biogeochemical tracers remains largely an open question.

4.2 Fronts as Regions of Exchange: Ekman Fluxes

Because it has been used primarily for studying frontal dynamics in the ocean interior, the kinematic framework has been most often deployed without consideration of wind-driven Ekman transport. However, Ekman advection is hypothesized to be a critical route by which nutrients enter into the subtropical gyres [12, 13] and cross the ACC to enrich the SAMW [14]. In the surface Ekman layer, a wind stress, τ , drives an Ekman transport, U_{Ek} , according to the Ekman relation:

$$U_{\text{Ek}} = -\hat{k} \times \frac{\tau}{\rho_o f} \quad (1)$$

where \hat{k} is the vertical coordinate, ρ_o is a reference density, and f is the Coriolis parameter. It is natural to speculate that Ekman transport across the subtropical-subpolar boundaries and the ACC should provide an important flux of nutrients to the equatorward side of these fronts. The location of these fronts is set by the zero contour of the wind stress curl. Where the wind stress curl vanishes, the along-front wind stress is maximized, as is the equatorward cross-stream Ekman transport it supports. Given the sharp increase in nutrients across the subtropical-subpolar and ACC fronts, described in Sect. 2, such Ekman transport is expected to provide a significant source of nutrients to the subtropics. A complication to this expectation is due to the effect of ocean eddies. Eddies provide a transfer of nutrients along isopycnals through familiar down-gradient eddy-induced diffusion, which augments the Ekman supply. However, eddies also transport mass due to the temporal correlation between anomalies of velocity on an isopycnal layer and the thickness of that layer [74]. The mass flux due to mesoscale motions is often called an ‘‘eddy bolus transport’’ and it can transfer nutrients either down-gradient or up-gradient [75]. This bolus transport has been shown to partially offset the Ekman transfer of nutrients across the ACC [17] and Gulf Stream [76] but enhance the offshore export of nutrients from eastern boundary upwelling regions [77]. In this section, we explore the strength of the global Ekman supply of nutrients alone and return to the question of the impact of eddies on nutrient transport in Sect. 4.3.

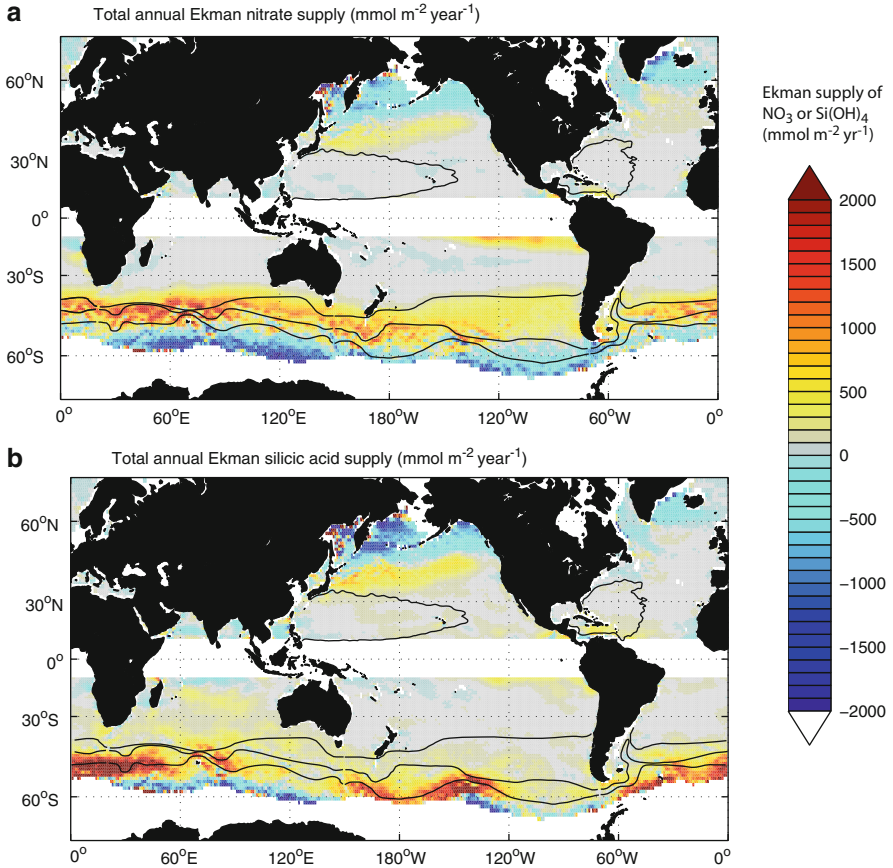


Fig. 13 Total annual Ekman supply of (a) nitrate and (b) silicic acid in $\text{mmol m}^{-2} \text{ year}^{-1}$ as deduced from the monthly satellite wind climatology of Risien and Chelton [78] and the World Ocean Atlas nutrient climatology [87], according to Eqs. (1 & 2) in the text. The averaging regions used for the budget calculations presented in Fig. 13 are outlined in black. In the Southern Ocean, these averaging regions are the Subantarctic Zone (bounded to the north by the Subtropical Front and to the south by the Subantarctic Front) and the Polar Frontal Zone (bounded to the north by the Subantarctic Front and the south by the Polar Front). These Southern Ocean Fronts are defined as in Belkin and Gordon [48]. In the Northern Hemisphere the averaging region is within the largest SSH contour encircling the gyres (1.71 m in the North Atlantic, and 2.12 m in the North Pacific). This contour is related to the largest closed surface geostrophic streamline of the anticyclonic circulation for the annual mean (differing by a factor of f , the Coriolis parameter)

The convergence of the Ekman nitrate and silicic acid transport, as deduced from an 8-year climatology of satellite wind stress [78] and a monthly nutrient climatology [79], confirms our expectation regarding the Ekman supply of nutrients: nitrate is exported from the subpolar surface ocean and converges in subtropical regions (Fig. 13). In the North Atlantic, the nutrient concentrations in the surface ocean are severely depleted, the Ekman supply of nitrate is low relative to the other basins, and

its influence extends over a limited region near the northern edge of the subtropical gyre. In contrast, the Pacific Ekman nitrate supply penetrates into the interior subtropical gyre. Ayers and Lozier [12] suggest that this Ekman nutrient supply governs the position of the Pacific transition zone chlorophyll front that extends into the central gyre [80]. In the Southern Ocean, a considerable Ekman supply of nitrate extends from the Antarctic Polar Front well into the subtropics. In contrast, the Ekman silicic acid supply is largely restricted to the Polar Frontal Zone, south of the SAF, where it converges in a narrower meridional band than the nitrate supply. This flux convergence is consistent with the hypothesis of silicic acid removal by diatom production and opal export north of the SAF [14, 15].

4.3 Ekman Fluxes in the Context of Other Nutrient Supply and Demand Terms

How does the cross-frontal Ekman transport compare with other physical and biological sources and sinks of nutrients? This question is best considered in the context of the steady state conservation equation for a nutrient (C) integrated over the annual maximum mixed layer depth (MLD):

$$\int_{z=-\text{MLD}}^0 \overset{1}{(\nabla \cdot \vec{u}C - \nabla \kappa_h \nabla C)} \overset{2}{\partial z} - \overset{3}{K_v \frac{\partial C}{\partial z}} \Big|_{z=-\text{MLD}} - \overset{4}{wC} \Big|_{z=-\text{MLD}} = \overset{5}{\int_{z=-\text{MLD}}^0 \text{SMS} \partial z} \quad (2)$$

Integrating over the annual maximum mixed layer eliminates the complication of resolving the seasonal redistribution of nutrients that are remineralized above this depth throughout the year and entrained into the mixed layer each winter (see [13] for a more detailed discussion of the limited role of local convection in maintaining euphotic zone nutrient concentrations). The terms of the equation are (1) the horizontal advective supply of the tracer above the annual maximum mixed layer depth; (2) the turbulent horizontal mixing of the tracer above the annual maximum mixed layer depth, parameterized here as a diffusive flux; (3) the mixing of the tracer across the base of the maximum mixed layer; (4) the vertical advection across the base of the maximum mixed layer; and (5) the biological source (remineralization of organic matter above the depth of the mixed layer) minus sink (export of organic matter across the base of the mixed layer). Because we integrate to the base of the annual maximum mixed layer, the only vertical fluxes that must be considered are the turbulent mixing supply (term 3), upwelling supply (term 4), and the flux of particulate nutrients across the base of that maximum mixed layer (in the source/sink term). To the degree that ocean biogeochemistry is in steady state on timescales of a year or more, a large influx of nutrients into the annually mixed layer should be balanced by the biological consumption and export

of these nutrients. Equivalently, a large nutrient outflux would imply the remineralization of organic nutrients.

Our goal is to perform an observationally based, order-of-magnitude assessment of the dominant supply mechanisms in the different regions for nitrate and silicic acid. To do so, we provide an approximation for as many of these terms as possible in the subtropical North Atlantic and North Pacific and in the Polar Frontal Zone and Subantarctic Zone of the Southern Ocean. The Ekman supply is embedded in term 1 of the conservation equation, as the mixed layer velocity is the sum of its Ekman and mean geostrophic components, as well as velocity arising from turbulent motion:

$$-\int_{z=-\text{MLD}}^0 \nabla \cdot \bar{u}C \partial z = -\nabla \cdot (U_{\text{Ek}}C_{\text{Ek}} + \langle \bar{u}_{\text{geo}}C \rangle H + \langle u^*C \rangle H) \quad (3)$$

Here we have decomposed the velocity into three components: U_{Ek} is the Ekman transport deduced from Eq. (1), which is vertically integrated over the Ekman layer; \bar{u}_{geo} is the time-mean geostrophic velocity; and u^* is the mean bolus velocity due to mesoscale motions including geostrophic turbulence [74]. In Eq. (3), H is the depth of the annual maximum mixed layer. The negative sign ensures that a nutrient supply is positive, i.e., transport convergence. The angled brackets represent the mean over the annual maximum mixed layer. C_{Ek} is a weighted average of the tracer concentration over the Ekman layer, with weights meant to mimic the velocity decay in the Ekman spiral. The weights are defined by an exponential decay with an e-folding scale of 22.1 m, as deduced from observations of velocity decaying in the Ekman spiral in the Drake Passage [81]. We note that because climatological nutrient concentrations are relatively homogenous in the upper 100 m of the ocean, our choice of e-folding depth only minimally impacts the Ekman supply term. Because the Ekman depth is generally above the annual maximum mixed layer depth, we make the reasonable assumption that the entire Ekman convergence is a supply term to this layer. The two-dimensional Ekman supply of nutrients is presented in Fig. 13, discussed in detail in Sect. 4.2. For the regions outlined in Fig. 13, we compare the annual Ekman supply to other terms in the conservation equation (Fig. 14). Because the Southern Ocean nutrient fluxes in the mixed layer are so much larger than those in the Northern subtropical gyres, they are plotted on separate scales.

The annual mean geostrophic transport at the ocean's surface is taken from Rio and Hernandez [23], which estimates the dynamic topography as the sum of sea-level anomalies averaged over the period 1992–2008 with a model of the geoid, constrained by observations. We have assumed that the surface geostrophic currents are uniform to the base of the annual maximum mixed layer, a simplification justified for our order-of-magnitude style analysis, as shallow mixed layers do not have the vertical distance for thermal wind shear to change the surface current significantly and deeper mixed layers are found in regions with weak stratification and more barotropic currents. The mixed layer depths are taken from the global 2° climatology constructed from hydrographic and Argo float profiles by de Boyer Montégut

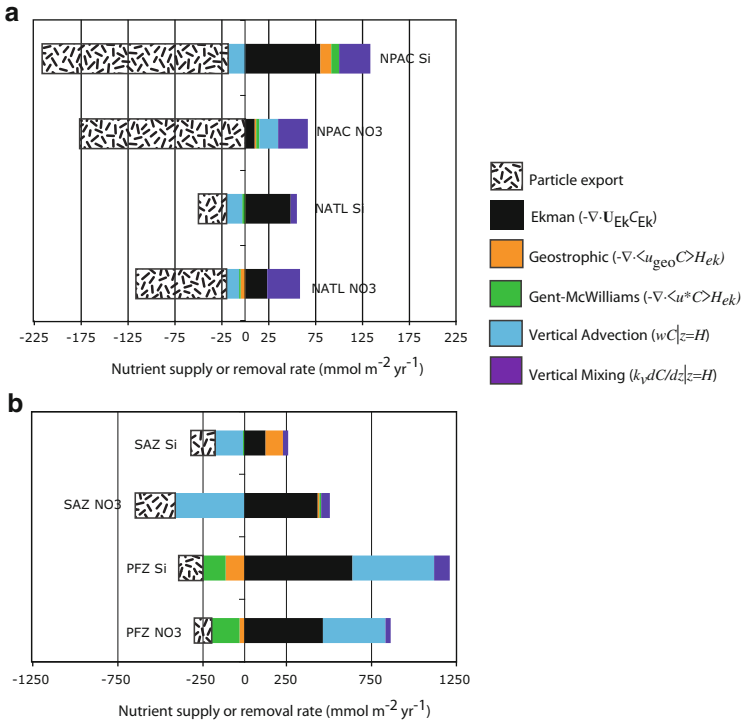


Fig. 14 The annual mean nitrate and silicic acid supply and removal rates ($\text{mmol m}^{-2} \text{year}^{-1}$) in the mixed layer of (a) North Atlantic and North Pacific and (b) the Southern Ocean Subantarctic Zone (SAZ) and Polar Front Zone (PFZ). The averaging region is outlined in Fig. 13. Note that the supply terms of nutrients in the Southern Ocean are roughly an order of magnitude greater than those in the Northern Hemisphere subtropical gyres. The calculation of each supply term is described in the text, along with an estimate of the uncertainty associated with each term, which is more than 50% of the estimated average value in many cases

et al. [82], recently updated to include profiles collected through 2008. While geostrophic currents are among the swiftest in the world ocean, these currents will only act as a supply term if the nutrient transport diverges, rather than simply recirculates around the gyres. Because the baroclinic component of the geostrophic flow is aligned with density fronts and density fronts coincide with nutrient fronts, the geostrophic flow is directed primarily along isolines of nutrients. This alignment would suggest small nutrient transport divergence for the time-mean geostrophic flow. However, our diagnostic of the divergence of geostrophic nutrient transport is not uniformly low; rather it is large and noisy. Thus, the mean geostrophic nutrient supply is very sensitive to the region over which it is averaged, and even the sign of this term is uncertain. In Fig. 14, the geostrophic term can be seen either as a supply or removal term.

The nutrient supply arising from mesoscale motions is also difficult to quantify since it depends on observations at fine spatial and temporal resolutions. As discussed

briefly in Sect. 4.2, eddies give rise to two tracer transport terms: one associated with a seawater mass flux ($\langle u^*C \rangle H$ in Eq. (3)) and the other associated with the turbulent mixing of the tracer with no corresponding seawater mass flux ($\int_{z=\text{MLD}}^0 \nabla \kappa_h \nabla C \partial z$ in Eq. (2)) [75]. Here, u^* represents the bolus velocity due to mesoscale eddies, flattening sloping isopycnals and therefore opposing the Ekman transport, which raises isopycnals in regions of Ekman divergence. Despite its critical role in tracer budgets [e.g., 83], the eddy bolus term is often neglected in observational studies because of chronically insufficient spatial and temporal sampling to directly observe the phenomenon.

To estimate the size of the eddy bolus nutrient supply, we make use of the Ocean Comprehensive Atlas (OCCA). OCCA is publicly available (<http://www.ecco-group.org/>) for the data-rich Argo period from 2004 to 2006 [84]. OCCA is an ocean climatology produced by calculating the least squares fit of the MIT general circulation model (MITgcm) to satellite and in situ data. A detailed description and validation of the global atlas, as well as applications for water mass formation studies in the Southern Ocean and North Atlantic, have demonstrated the skill and utility of this framework [84, 85]. The MITgcm uses the Gent and McWilliams (GM) formulation (with a thickness diffusion coefficient of $1,000 \text{ m}^2 \text{ s}^{-1}$) to parameterize the bolus velocities arising from mesoscale motions [86], and these velocities are included in the OCCA. We multiply these GM velocities by the lateral nutrient gradients from World Ocean Atlas [87]. A limitation of this framework is that it neglects spatial gradients in the diffusion coefficient, though these gradients can be substantial across fronts, as elucidated by the kinematic studies discussed in Sect. 4.1. Averaged over the North Pacific and North Atlantic Subtropical gyres, the GM term is much smaller than the other terms (Fig. 14). In both the Polar Frontal Zone and the Subantarctic Zone, the nutrient transport due to the GM velocities clearly opposes the Ekman nutrient transport. This opposition is expected given that Ekman transport tends to tilt isopycnals into the vertical, whereas the net effect of eddies is to lay the isopycnals flat. Our scale analysis suggests that, in the Polar Frontal Zone, the removal of nitrate by the GM term is of the same order and opposite sign as the Ekman supply term. For other all other fronts, the estimate for the GM term is an order of magnitude smaller than the Ekman term.

The last of the lateral supply terms, the turbulent mixing of tracers, is often parameterized as the Laplacian diffusion of the tracer as depicted in term 2 of Eq. (2). This term can be scaled as $\kappa_h \left(\frac{\Delta_x C}{L_x^2} + \frac{\Delta_y C}{L_y^2} \right) H$. Values of κ_h are generally $1,000 \text{ m}^2 \text{ s}^{-1}$ or lower [88], but are thought to be four times smaller across the barrier regions of fronts [5]. Recalling Fig. 2, we can see that the maximum change in nitrate and silicic acid is about 3 mmol m^{-3} and 6 mmol m^{-3} , respectively, over a length scale of 100 km at the edges of the Northern Hemisphere subtropical gyres. Integrating over an annual maximum mixed layer depth of 250 m and applying a mixing coefficient, κ_h , of $250 \text{ m}^2 \text{ s}^{-1}$, we arrive at a lateral mixing supply on the order of several hundred $\text{mmol m}^{-2} \text{ year}^{-1}$ in the high-gradient region at the front. Because the high-gradient region is restricted to the gyre's edges, the diffusive supply averaged over the entire gyre is at least one to two orders of magnitude

smaller than this estimate for the region near the front. For values more appropriate to the ACC of $L_y = 1,000$ km, $\Delta_y \text{NO}_3 = 25$ mmol m⁻³, and $\Delta_x \text{NO}_3 = 0$ mmol m⁻³ and mixed layer of 400 m, the down-gradient diffusion is on the order of 100 mmol m⁻² year⁻¹. Thus, the lateral mixing supply is likely a significant nutrient source for the low-nutrient subtropics near their boundaries.

Our scale analysis of the lateral mixing supply is highly sensitive to the choice of diffusion coefficients, which may vary significantly between the frontal regions where nutrient concentrations change rapidly and the homogenous region between the fronts [88]. Characterizing the entire region by one value of κ_h and one length scale ignores the fact that most of the horizontal change in nutrient concentrations happens over a narrow region near the front where horizontal mixing is inhibited. Given these caveats, this term is uncertain even in its order of magnitude, and is therefore excluded from Fig. 14. The mixing of tracers is a ripe area for future research, and eddy-resolving models are rapidly challenging how we conceptualize the influence of mesoscale motions on frontal dynamics [89], tracer budgets [73, 75], and biogeochemistry [90].

Having tackled the lateral supply terms, we turn our attention to the vertical supply. The vertical mixing term (term 3 in Eq. (2)) is calculated from the nutrient gradient from the World Ocean Atlas [87] interpolated to the depth of the annual maximum mixed layer depth from de Boyer Montégut et al. [82] and multiplied by a typical upper open-ocean value of $\kappa_v = 4 \times 10^{-5}$ m² s⁻¹ [91–94]. Often considered the dominant supply term of nutrients to the surface of the subtropical gyres, this analysis suggests that the vertical mixing flux is no bigger than the Ekman supply in these regions (Fig. 13). However, this rough scaling of the vertical mixing is also subject to considerable uncertainty, as the vertical mixing coefficient is subject to spatial and temporal variability [95, 96].

The last physical supply term, the vertical advection of nutrients (term 4 in Eq. (2)) is estimated from the vertical velocities from the OCCA multiplied by the climatological mean nutrient concentration [79] at the base of the de Boyer Montégut [82] maximum mixed layer depth. OCCA incorporates the observed winds into a model with full physics and therefore simulates vertical velocities resulting from wind forcing along with other sources of vertical motion. As expected for the downwelling gyres of the subtropical North Atlantic and North Pacific, vertical advection generally removes nutrients from the surface mixed layer (Fig. 14). Likewise in the Subantarctic Zone, where the wind stress curl promotes downwelling conditions, nutrients are removed from the surface mixed layer by vertical advection. On the other hand, the Polar Frontal Zone, poleward of the zero wind stress curl line, receives an enormous upwelling supply of nitrate and silicic acid. The upwelling supply of nitrate dominates all other supply terms in the PFZ. In contrast, the Ekman supply of silicic acid to the PFZ is comparable to the upwelling supply, because of the rapid convergence of silicic acid in the PFZ (Fig. 13).

Finally, we examine the export of particulate organic nitrogen and silica across the base of the annual maximum mixed layer depth (term 5 in Eq. (2)) for each region. The export of nutrients from the euphotic zone (nominally 75 m) has been provided by John Dunne from his work using empirical relationships to deduce the

global export of organic matter from satellite data [29]. We propagate the export of nutrients to the depth of the annual maximum mixed layer depth with the Martin formulation: $F(z) = F_{75} \times (z/75)^{-0.9}$, where $F(z)$ is the export as a function of depth and F_{75} is the export at 75 m.

It is tempting to speculate about the mismatches between nutrient supply and demand terms in Fig. 14 and search for sources or sinks to close the gap. However, these mismatches are very likely smaller than the sum of uncertainties on each term, the calculation of which is far from straightforward. Of the physical terms that are depicted in Fig. 14, the geostrophic nutrient supply may have the largest percent errors. The satellite-derived geostrophic velocities have an RMS error relative to drifters of 10–15 cm s⁻¹ in swift boundary currents and 3–5 cm s⁻¹ in low variability areas [23], which is between 10 and 100% of the mean velocities. The size of the geostrophic term is also very sensitive to averaging region. In addition, the annual mean nitrate concentrations in World Ocean Atlas have an average standard error of 7% of mean concentration in the top 500 m of the water column [87]. The eddy-driven advection of nutrients is also uncertain, in large part because of our choice of a constant GM diffusion coefficient of 1,000 m² s⁻¹. A recent statistical analysis of surface drifters and satellite altimetry suggests that average cross-ACC diffusion near the Polar Front is between 2,000 and 4,000 m² s⁻¹ [97]. A higher diffusion coefficient would translate to a stronger eddy transport of nutrients out of the Polar Frontal Zone, helping offset the huge vertical supply. Uncertainties associated with the organic particle sinking flux are also considerable; these are derived from a multistep process accounting for known and unknown errors at each step, leading to an estimated 40% uncertainty in the export of organic carbon [29]. In addition, to convert the total export of organic carbon to nutrient export, spatially variable stoichiometric ratios are used, introducing an additional error of up to 4% [29]. Thus, the error for the estimate of nutrient export is of the order 50%.

In addition to the errors on the terms appearing in Fig. 14, there are terms that are neglected entirely in this depiction. First, our scale analysis of mixing of nutrients across the fronts was too uncertain to be included in Fig. 14. Next, the eddy heaving of isopycnals laden with nutrients into the euphotic zone, while not being part of the diapycnal mixing term, has been invoked to close the nutrient budget [98], though a quantitative estimate of this supply mechanism remains controversial [99]. Moreover, the eddy heaving hypothesis does not explain the summertime drawdown of dissolved inorganic carbon that occurs in the absence of a corresponding inorganic nutrient drawdown, observed at the Bermuda Atlantic Time Series and the Hawaii Ocean Time Series [100]. Models and observations have suggested an important role for dissolved organic nutrients in fueling subtropical productivity [101–104], which would help explain carbon fixation in the absence of inorganic nutrient drawdown. Nutrients in their dissolved organic form persist in the euphotic zone longer than their inorganic counterparts. In theory, the conversion of particulate organic matter to dissolved organic matter would allow the cross-frontal flux of nutrients to persist further from the fronts, since it effectively lengthens the time-scale for the particles to sink past the base of the mixed layer. Finally, nitrogen

fixation may provide a complementary biological mechanism capable of supplying fixed nitrogen to the subtropical gyres [e.g., 76, 105, 106], as long as phosphate and iron are available.

Despite large uncertainties in the scale analysis of nutrient supply and demand, Fig. 14 suggests two salient messages. First, lateral processes provide critical supply terms of nutrients in both the Northern Hemisphere subtropical gyres and the downwelling Subantarctic Zone of the Southern Hemisphere. Thus, we should abandon any expectation that the vertical sinking of particles be balanced locally by vertical transport processes. Second, the search for a missing nutrient supply in the subtropics [e.g., 94] might be more accurately reframed as a quest for smaller errors and particularly better constraints on the turbulent mixing supply across the gyre's bounding fronts. The sign of the imbalances in the Southern Ocean especially suggest this to be an area of needed improvement: the down-gradient transport of nutrients from the PFZ to the SAZ would bring our scale analysis closer to balance in both regions.

5 Conclusions and Open Questions

In our tour of the ocean's large-scale biogeochemical fronts, we first discussed the processes that maintain these sharp gradient regions and then explored the mechanisms that act against them. We have shown that, on timescales greater than a year, cross-frontal exchange plays a critical role in fueling primary productivity in the vertically stratified and laterally homogenous subtropical regions. Though diffusivity across density fronts is often reduced relative to background diffusivity, the exchange that is permitted acts on a sharp biogeochemical gradient, thus reconciling the apparently disparate views of fronts as both barriers to mixing and essential gateways of exchange.

Ekman transport proves to be a powerful exchange mechanism across the boundaries of the subtropical gyres, particularly at their poleward flanks, and is a crucial supplier of nutrients to the subtropics, as first revealed for the subtropical North Atlantic by Williams and Follows [13]. The Ekman supply is also easy to diagnose, requiring only knowledge of wind stress and nutrient concentrations. We suspect that isopycnal mixing due to mesoscale motions is also an important term in nutrient budgets. However, there are still relatively few observations or models that resolve the spatial scale at which this exchange happens (tens of kilometers) and can simultaneously quantify the impact at basin to global scales. The parameterizations of isopycnal mixing in the coarse-resolution models used to simulate climate and biogeochemistry generally do not include the impact of jets on the suppression of isopycnal mixing at the jet core and the enhancement along critical levels. Thus, the quantitative role of mixing across fronts remains an open frontier for exploration in terms of its biogeochemical impact. Moreover, this exploration is becoming timely given both that parameterizations of isopycnal mixing more accurately reflecting jet dynamics are rapidly evolving [e.g., 107] and that the use of eddy-resolving models for biogeochemical studies is now feasible.

In the Northern Hemisphere subtropics, our estimate of the nutrient supply rate is within the (large) errors of estimate of the nutrient demand. As more robust estimates of isopycnal mixing, the vertical eddy supply of nutrients, nitrogen fixation, and primary productivity fueled by dissolved organic nutrients become available, we expect these budgets to approach a more quantitative balance. In the mixed layer of the downwelling Subantarctic Zone, nutrient concentrations are much higher than in the Northern Hemisphere subtropics. Here, the Ekman flux of nutrients across the Subantarctic Front is balanced in large part by the downwelling of nutrients from the mixed layer into the pycnocline. This balance underscores the role of the ACC fronts as nutrient gateways. Between the Polar Front and Subantarctic Front, powerful westerly winds drive the upwelling of nutrients from the abyss; Ekman transport drives these nutrients across the Subantarctic Front; and north of the Subantarctic Front, these nutrients are pumped into the pycnocline. Thus, the fronts of the ACC provide a critical connection between the dense ocean interior and the pycnocline. Without this link, the nutrients that sink past the base of the pycnocline would depend entirely on diapycnal mixing to make their upward return trip, and the global distribution of productivity would be significantly altered [16].

Even as we seek a fundamental understanding of the role of cross-frontal processes in setting annual mean nutrient budgets, intriguing questions about the temporal variability of these processes are on the horizon. Variability in Ekman exchange across fronts, which is largely modulated by variability in wind stress, influences seasonality in chlorophyll concentrations in the subtropical North Pacific [12]. In addition, intra-annual variability in the cross-ACC flux of biogeochemical tracers appears to be tied to Ekman transport variability with little compensation by eddy advection [90]. However, connections between cross-frontal Ekman transport and subtropical biogeochemical variability have yet to be fully explored on inter-annual or interdecadal timescales. Similarly, recent observations have revealed substantial interannual variability in the shallow limb of the Meridional Overturning Circulation (MOC) [108, 109], which is an important conduit of nutrients to the North Atlantic [36, 37, 45, 110]. Yet, a quantitative assessment of impact of MOC's variability on the biogeochemistry of the North Atlantic awaits future study. Likewise, in the North Pacific, ring-mediated exchange across the Kuroshio is hypothesized to set interannual variability in the density stratification of the subtropical mode water in the North Pacific [42, 43], but the implications for nutrients and phytoplankton remain largely unexplored. Deploying our physical understanding of cross-frontal exchange to answer these unresolved questions about the living ocean offers a wealth of prospects for future research.

Acknowledgements The authors are grateful to Stephanie Schollaert-Uz, Ric Williams, and Igor Belkin for insightful reviews, which improved an early draft of this chapter. We thank John Dunne for his use of the particulate nutrient export data. We also gratefully acknowledge the many data and modeling resources used throughout this work that have been made available online: the AVISO group for compiling and making available satellite altimetry data and related products; the Estimating the Circulation and Climate of the Ocean (ECCO) group for publishing several versions of the ECCO model output, including the Ocean Circulation on Climate Atlas (OCCA) used here; de Boyer Montegut and colleagues who have calculated mixed layer depths for the

global ocean and continue updating the calculations with ARGO data; Risien and Chelton who have posted their climatology of global wind stress; and the NODC for publishing the World Ocean Atlas. Support from the Canada's NSERC Discovery program, NOAA-Cooperative Institute for Climate Science Grant #NA08OAR4320752; the National Oceanic and Atmospheric Administration, US Department of Commerce award NA07OAR4310096; and the Office of Science (BER), US Department of Energy, Grant No. DE-FG02-07ER64467 are gratefully acknowledged. This material is based upon work partially supported by the National Science Foundation under Grant No. 0701252. All statements, findings, conclusions, and recommendations are those of the authors and do not necessarily reflect the views of the National Oceanic and Atmospheric Administration, the US Department of Commerce, the US Department of Energy, NSERC, or the National Science Foundation.

References

1. Hoskins BJ (1982) The mathematical theory of frontogenesis. *Annu Rev Fluid Mech* 14(1): 131–151. doi:[10.1146/annurev.fl.14.010182.001023](https://doi.org/10.1146/annurev.fl.14.010182.001023)
2. Rhines P (1994) Jets. *Chaos: an interdisciplinary. J Nonlinear Sci* 4(2):313–339
3. Rudnick D, Ferrari R (1999) Compensation of horizontal temperature and salinity gradients in the ocean mixed layer. *Science* 283:526–529
4. Macvean MK, Woods JD (1980) Redistribution of scalars during upper ocean frontogenesis: a numerical model. *QJR Meteorol Soc* 106:293–311. doi:[10.1002/qj.49710644805](https://doi.org/10.1002/qj.49710644805)
5. Bower AS, Rossby HT, Lillibridge JL (1985) The gulf stream: barrier or blender? *J Phys Oceanogr* 15:24–32
6. Bower AS (1991) A simple kinematic mechanism for mixing fluid parcels across a meandering jet. *J Phys Oceanogr* 21:173–180
7. Bower AS, Lozier MS (1994) A closer look at particle exchange in the gulf stream. *J Phys Oceanogr* 24(6):1399–1418. doi:[10.1175/1520-0485\(1994\)024<1399:ACLAPE>2.0.CO;2](https://doi.org/10.1175/1520-0485(1994)024<1399:ACLAPE>2.0.CO;2)
8. Williams RG, Follows MJ (2003) Physical transport of nutrients and the maintenance of biological production. In: Fasham MJR (ed) *Ocean biogeochemistry*. Springer-Verlag, Berlin, pp 19–51
9. Klaas C, Archer DE (2002) Association of sinking organic matter with various types of mineral ballast in the deep sea: implications for the rain ratio. *Global Biogeochem Cycles* 16(4): 63–61
10. Lutz M, Dunbar R, Caldeira K (2002) Regional variability in the vertical flux of particulate organic carbon in the ocean interior. *Global Biogeochem Cycles* 16(3):11–18
11. Martin JH, Knauer GA, Karl DM, Broenkow WW (1987) VERTEX: carbon cycling in the northeast Pacific. *Deep Sea Res A Oceanogr Res Pap* 34(2):267–285
12. Ayers J, Lozier M (2009) Physical controls on the seasonal migration of the North Pacific Transition Zone Chlorophyll Front. *J Geophys Res*. doi:[10.1029/2009JC005596](https://doi.org/10.1029/2009JC005596)
13. Williams RG, Follows MJ (1998) The Ekman transfer of nutrients and maintenance of new production over the North Atlantic. *Deep Sea Res I Oceanogr Res Pap* 45(2–3):461–489
14. Sarmiento JL, Gruber N, Brzezinski MA, Dunne JP (2004) High-latitude controls of thermocline nutrients and low latitude biological productivity. *Nature* 427:56–60
15. Sarmiento JL, Simeon J, Gnanadesikan A, Gruber N, Key RM, Schlitzer R (2007) Deep ocean biogeochemistry of silicic acid and nitrate. *Global Biogeochem Cycles* 21(1):GB1S90
16. Gnanadesikan A, Dunne JP, Key RM, Matsumoto K, Sarmiento JL, Slater RD, Swathi PS (2004) Oceanic ventilation and biogeochemical cycling: understanding the physical mechanisms that produce realistic distributions of tracers and productivity. *Global Biogeochem Cycles* 18(4): 1–17
17. Palter JB, Sarmiento J, Gnanadesikan A, Simeon J, Slater R (2010) Fueling export production: nutrient return pathways from the deep ocean and their dependence on the Meridional Overturning Circulation. *Biogeosciences* 7(11):3549–3568. doi:[10.5194/bg-7-3549-2010](https://doi.org/10.5194/bg-7-3549-2010)

18. Tomczak M, Godfrey J (2003) *Regional oceanography: an introduction*, 2nd edn. Pergamon, New York
19. Sharples J, Simpson J (2001) Shelf sea and shelf slope fronts. In: Steele JH, Thorpe SA, Turekian KK (eds) *Encyclopedia of ocean sciences*. Academic, San Diego, pp 2760–2768
20. Simpson J (1998) Tidal processes in shelf seas. In: Brink KH, Robinson AR (eds) *The sea*, vol 10. Wiley, New York
21. Luyten J, Pedlosky J, Stommel H (1983) The ventilated thermocline. *J Phys Oceanogr* 13:292–309
22. Pedlosky J (1990) The dynamics of the oceanic subtropical gyres. *Science* 248:316–322
23. Rio MH, Hernandez F (2004) A mean dynamic topography computed over the world ocean from altimetry, in situ measurements, and a geoid model. *J Geophys Res* 109(C12), C12032. doi:[10.1029/2003jc002226](https://doi.org/10.1029/2003jc002226)
24. Fine RA, Maillet KA, Sullivan KF, Willey D (2001) Circulation and ventilation flux of the Pacific Ocean. *J Geophys Res* 106. doi:[10.1029/1999jc000184](https://doi.org/10.1029/1999jc000184)
25. Sarmiento JL (1983) A tritium box model of the North Atlantic thermocline. *J Phys Oceanogr* 13(7):1269–1274
26. Jenkins WJ, Wallace DWR (1992) Tracer based inferences of new primary production in the sea. In: Falkowski PG, Woodhead AD (eds) *Primary productivity and biogeochemical cycles in the sea*, vol 37. Springer, Plenum, New York, pp 299–316
27. McCartney MS (1982) The subtropical recirculation of Mode Waters. *J Mar Res* 40:427–464
28. Stommel H (1979) Determination of water mass properties of water pumped down from the Ekman layer to the geostrophic flow below. *Proc Natl Acad Sci* 76:3051–3055
29. Dunne JP, Sarmiento JL, Gnanadesikan A (2007) A synthesis of global particle export from the surface ocean and cycling through the ocean interior and on the seafloor. *Global Biogeochem Cycles* 21(4):16
30. Sarmiento JL, Herbert TD, Toggweiler JR (2008) Causes of anoxia in the world ocean. *Global Biogeochem Cycles* 2. doi:[10.1029/GB002i002p00115](https://doi.org/10.1029/GB002i002p00115)
31. Najjar RG, Sarmiento JL, Toggweiler JR (1992) Downward transport and fate of organic matter in the ocean: simulations with a general circulation model. *Global Biogeochem Cycles* 6. doi:[10.1029/91gb02718](https://doi.org/10.1029/91gb02718)
32. Palter JB, Lozier MS, Barber RT (2005) The effect of advection on the nutrient reservoir in the North Atlantic subtropical gyre. *Nature* 437(7059):687–692
33. Brandt P, Hormann V, Körtzinger A, Visbeck M, Krahnemann G, Stramma L, Lumpkin R, Schmid C (2010) Changes in the ventilation of the oxygen minimum zone of the Tropical North Atlantic. *J Phys Oceanogr* 40(8):1784–1801. doi:[10.1175/2010JPO4301.1](https://doi.org/10.1175/2010JPO4301.1)
34. Deutsch C, Sigman DM, Thunell RC, Meckler AN, Haug GH (2004) Isotopic constraints on glacial/interglacial changes in the oceanic nitrogen budget. *Global Biogeochem Cycles* 18(4): 1–22
35. Gruber N, Sarmiento JL (1997) Global patterns of marine nitrogen fixation and denitrification. *Global Biogeochem Cycles* 11(2):235–266
36. Moore CM, Mills MM, Achtenberg EP, Geider RJ, Laroche J, Lucas MI, McDonagh EL, Pan X, Poulton AJ, Rijkenberg MJA, Suggett DJ, Ussher SJ, Woodward EMS (2009) Large-scale distribution of Atlantic nitrogen fixation controlled by iron availability. *Nat Geosci* 2(12): 867–871
37. Williams RG, Roussenov V, Follows MJ (2006) Nutrient streams and their induction into the mixed layer. *Global Biogeochem Cycles* 20(1):GB1016. doi:[10.1029/2005gb002586](https://doi.org/10.1029/2005gb002586)
38. Lewis MR, Kuring N, Yentsch C (1988) Global patterns of ocean transparency: implications for the new production of the open ocean. *J Geophys Res* 93(C6):6847–6856
39. Follows MJ, Dutkiewicz S (2002) Meteorological modulation of the North Atlantic spring bloom. *Deep Sea Res II* 49:321–344
40. Sverdrup H (1953) On conditions for the vernal blooming of phytoplankton. *J Int Council Exploration Sea* 18:287–295
41. Broecker WS, Peng T-H (1982) *Tracers in the Sea*. Lamont-Doherty Earth Observatory, Palisades

42. Qiu B, Chen S, Hacker P (2007) Effect of mesoscale eddies on subtropical mode water variability from the Kuroshio Extension System Study (KESS). *J Phys Oceanogr* 37(4): 982–1000
43. Qiu B, Chen S (2006) Decadal variability in the formation of the North Pacific subtropical mode water: oceanic versus atmospheric control. *J Phys Oceanogr* 36(7):1365–1380
44. Wiggins S (2005) The dynamical systems approach to Lagrangian transport in oceanic flows. *Annu Rev Fluid Mech* 37:295–328
45. Palter JB, Lozier MS (2008) On the source of Gulf Stream nutrients. *J Geophys Res* 113: C06018
46. Tsuchiya M (1989) Circulation of the Antarctic intermediate water in the North Atlantic Ocean. *J Mar Res* 47:747–755
47. Williams RG, McDonagh EL, Roussenov VM, Torres-Valdes S, King B, Sanders R, Hansell DA (2011) Nutrient streams in the North Atlantic: advective pathways of inorganic and organic nutrients. *Global Biogeochem Cycles* 25(GB4008). doi:[10.1029/2010GB003853](https://doi.org/10.1029/2010GB003853)
48. Belkin IM, Gordon AL (1996) Southern Ocean fronts from the Greenwich meridian to Tasmania. *J Geophys Res C Oceans* 101(C2):3675–3696
49. Deacon GER (1937) The hydrology of the Southern Ocean. *Discovery Rep* 15:1–124
50. Orsi AH, Whitworth T, Nowlin WD (1995) On the meridional extent and fronts of the Antarctic Circumpolar Current. *Deep Sea Res I Oceanogr Res Pap* 42(5):641–673
51. Sokolov S, Rintoul SR (2009) Circumpolar structure and distribution of the Antarctic Circumpolar Current fronts: 1. Mean circumpolar paths. *J Geophys Res* 114(19). doi:[10.1029/2008JC005108](https://doi.org/10.1029/2008JC005108)
52. Hughes CW, Ash ER (2001) Eddy forcing of the mean flow in the Southern Ocean. *J Geophys Res* 106(C2):2713–2722. doi:[10.1029/2000jc900332](https://doi.org/10.1029/2000jc900332)
53. Naveira Garabato AC, Jullion LØ, Stevens DP, Heywood KJ, King BA (2009) Variability of subantarctic mode water and Antarctic intermediate water in the drake passage during the late-twentieth and early-twenty-first centuries. *J Climate* 22(13):3661–3688. doi:[10.1175/2009jcli2621.1](https://doi.org/10.1175/2009jcli2621.1)
54. Sokolov S, Rintoul SR (2007) On the relationship between fronts of the Antarctic Circumpolar Current and surface chlorophyll concentrations in the Southern Ocean. *J Geophys Res* 112. doi:[10.1029/2006jc004072](https://doi.org/10.1029/2006jc004072)
55. Pollard R, Lucas M, Read J (2002) Physical controls on biogeochemical zonation in the Southern Ocean. *Deep Sea Res II* 49:3289–3305
56. Whitworth T, III, Orsi AH, Kim SJ, Nowlin WD, Jr, Locarnini RA (1998) Water masses and mixing near the Antarctic slope front. In: *Ocean, ice, and atmosphere: interactions at the antarctic continental margin*, vol 75. Antarctic Research Series, AGU, Washington, pp 1–27
57. Jacobs SS (1991) On the nature and significance of the Antarctic Slope Front. *Mar Chem* 35 (1–4):9–24. doi:[10.1016/S0304-4203\(09\)90005-6](https://doi.org/10.1016/S0304-4203(09)90005-6)
58. Mosby H (1934) The waters of the Atlantic Antarctic Ocean. In: Dybwad J (ed) *Scientific results of The Norwegian Antarctic Expeditions 1927–1928*, vol 11. Consul Lars Christensen, Oslo
59. Boyd P, LaRoche J, Gall M, Frew R, McKay RML (1999) Role of iron, light, and silicate in controlling algal biomass in subantarctic waters SE of New Zealand. *J Geophys Res Oceans* 104(C6):13395–13408. doi:[10.1029/1999jc900009](https://doi.org/10.1029/1999jc900009)
60. Marinov I, Gnanadesikan A, Toggweiler JR, Sarmiento JL (2006) The Southern Ocean biogeochemical divide. *Nature* 441(7096):964–967
61. Takeda S (1998) Influence of iron availability on nutrient consumption ratio of diatoms in oceanic waters. *Nature* 393(6687):774–777
62. Leynaert A, Bucciarelli E, Claquin P, Dugdale RC, Martin-Jézéquel V, Pondaven P, Ragueneau O (2004) Effect of iron deficiency on diatom cell size and silicic acid uptake kinetics. *Limnol Oceanogr* 49(4I):1134–1143
63. Franck VM, Brzezinski MA, Coale KH, Nelson DM (2000) Iron and silicic acid concentrations regulate Si uptake north and south of the Polar Frontal Zone in the Pacific Sector of the Southern Ocean. *Deep Sea Res II Topical Studies Oceanogr* 47(15–16): 3315–3338

64. Matsumoto K, Sarmiento, JL, Brzezinski MA (2002) Silicic acid leakage from the Southern Ocean: a possible explanation for glacial atmospheric pCO₂. *Global Biogeochem. Cycles* 16. doi:[10.1029/2001gb001442](https://doi.org/10.1029/2001gb001442)
65. Brzezinski MA, Pride CJ, Franck VM, Sigman DM, Sarmiento JL, Matsumoto K, Gruber, N, Rau GH, Coale KH (2002) A switch from Si(OH)₄ to NO₃ depletion in the glacial Southern Ocean. *Geophys Res Lett* 29(12). doi:[10.1029/2001gl014349](https://doi.org/10.1029/2001gl014349)
66. Ito T, Follows MJ (2005) Preformed phosphate, soft tissue pump and atmospheric CO₂. *J Mar Res* 63(4):813–839
67. Marinov I, Gnanadesikan A, Sarmiento JL, Toggweiler JR, Follows M, Mignone BK (2008) Impact of oceanic circulation on biological carbon storage in the ocean and atmospheric pCO₂. *Global Biogeochem Cycles* 22(3):GB3007
68. Marinov, I., Follows, M.J., Gnanadesikan, A., Sarmiento, J.L., Slater, R.D.: How does ocean biology affect atmospheric pCO₂? Theory and models. *Journal of Geophysical Research C: Oceans* 113(7) (2008).
69. Archer DE, Eshel G, Winguth A, Broecker W, Pierrehumbert R, Tobis M, Jacob R (2000) Atmospheric pCO₂ sensitivity to the biological pump in the ocean. *Global Biogeochem Cycles* 14(4):1219–1230
70. Rogerson A, Miller P, Pratt L, Jones C (1999) Lagrangian motion and fluid exchange in a barotropic meandering jet. *J Phys Oceanogr* 29:2635–2655
71. Samelson RM (1992) Fluid exchange across a meandering jet. *J Phys Oceanogr* 22:431–440
72. Lozier M, Pratt L, Rogerson A, Miller P (1997) Exchange geometry revealed by float trajectories in the Gulf Stream. *J Phys Oceanogr* 27:2327–2341
73. Abernathy R, Marshall J, Mazloff M, Shuckburgh E (2010) Enhancement of mesoscale eddy stirring at steering levels in the Southern Ocean. *J Phys Oceanogr* 40(1):170–184. doi:[10.1175/2009JPO4201.1](https://doi.org/10.1175/2009JPO4201.1)
74. Gent PR, Willebrand J, McDougall TJ, McWilliams JC (1995) Parameterizing eddy-induced tracer transports in ocean circulation models. *J Phys Oceanogr* 25(4):463–474
75. Lee MM, Williams RG (2000) The role of eddies in the isopycnic transfer of nutrients and their impact on biological production. *J Mar Res* 58(6):895–917
76. Palter JB, Lozier MS, Sarmiento JL, Williams RG (2011) The supply of excess phosphate across the Gulf Stream and the maintenance of subtropical nitrogen fixation. *Global Biogeochem Cycles* 25(4), GB4007. doi:[10.1029/2010gb003955](https://doi.org/10.1029/2010gb003955)
77. Gruber N, Lachkar Z, Frenzel H, Marchesiello P, Munnich M, McWilliams JC, Nagai T, Plattner G-K (2011) Eddy-induced reduction of biological production in eastern boundary upwelling systems. *Nature Geosci* 4(11):787–792
78. Risien CM, Chelton DB (2008) A global climatology of surface wind and wind stress fields from eight years of QuikSCAT scatterometer data. *J Phys Oceanogr* 38(11):2379–2413
79. Conkright ME, Locarnini RA, Garcia HE, O'Brien TD, Boyer TP, Stephens C, Antonov JI (2001) World Ocean Atlas 2001: objective analyses, data statistics, and figures. In: National Oceanographic Data Center, Silver Spring, p 17
80. Polovina JJ, Howell E, Kobayashi DR, Seki MP (2001) The transition zone chlorophyll front, a dynamic global feature defining migration and forage habitat for marine resources. *Prog Oceanogr* 49(1–4):469–483
81. Lenn YD, Chereskin TK (2009) Observations of Ekman currents in the Southern Ocean. *J Phys Oceanogr* 39(3):768–779
82. de Boyer Montégut C, Madec G, Fischer AS, Lazar A, Iudicone D (2004) Mixed layer depth over the global ocean: an examination of profile data and a profile-based climatology. *J Geophys Res Oceans* 109(C12), C12003. doi:[10.1029/2004jc002378](https://doi.org/10.1029/2004jc002378)
83. Danabasoglu G, McWilliams JC, Gent PR (1994) The role of mesoscale tracer transports in the global ocean circulation. *Science* 264(5162):1123–1126
84. Forget G (2009) Mapping ocean observations in a dynamical framework: a 2004–2006 ocean atlas. *J Phys Oceanogr* 40(2010):1201–1221

85. Maze G, Forget G, Buckley M, Marshall J, Cerovecki I (2009) Using transformation and formation maps to study the role of air-sea heat fluxes in North Atlantic Eighteen Degree Water Formation. *J Phys Oceanogr* 39(8):1818–1835
86. Gent PR, McWilliams JC (1990) Isopycnal mixing in ocean circulation models. *J Phys Oceanogr* 20:150–155
87. Garcia HE, Locarnini RA, Boyer TP, Antonov JI, Zweng MM, Baranova OK, Johnson DR (2010) World Ocean Atlas 2009, Volume 4: Nutrients (phosphate, nitrate, silicate). In: Levitus S (ed) NOAA Atlas NESDIS 71, vol 4. U.S. Government Printing Office, Washington, p 398
88. Visbeck M, Marshall J, Haine T, Spall M (1997) Specification of eddy transfer coefficients in coarse-resolution ocean circulation models. *J Phys Oceanogr* 27:381–402
89. Hallberg R, Gnanadesikan A (2006) The role of eddies in determining the structure and response of the wind-driven southern hemisphere overturning: results from the modeling eddies in the southern ocean (MESO) project. *J Phys Oceanogr* 36(12):2232–2252
90. Ito T, Woloszyn M, Mazloff M (2010) Anthropogenic carbon dioxide transport in the Southern Ocean driven by Ekman flow. *Nature* 463(7277):80–83
91. Winkel DP, Gregg MC, Sanford TB (2002) Patterns of shear and turbulence across the Florida Current. *J Phys Oceanogr* 32(11):3269–3285
92. Ledwell JR, Watson AJ, Law CS (1993) Evidence for slow mixing across the pycnocline from an open-ocean tracer-release experiment. *Nature* 364:701–703
93. Gregg MC, Sanford TB (1980) Signatures of mixing from the Bermuda Slope, the Sargasso Sea and the Gulf Stream. *J Phys Oceanogr* 10:105–127
94. Lewis MR, Harrison WG, Oakey NS, Hebert D, Platt T (1986) Vertical nitrate fluxes in the oligotrophic ocean. *Science* 234:870–873
95. Naveira Garabato AC, Polzin KL, King BA, Heywood KJ, Visbeck M (2004) Widespread intense turbulent mixing in the Southern Ocean. *Science* 303(5655):210–213
96. Heywood KJ, Naveira Garabato AC, Stevens DP (2002) High mixing rates in the abyssal Southern Ocean. *Nature* 415(6875):1011–1014
97. Sallée JB, Speer K, Morrow R, Lumpkin R (2008) An estimate of Lagrangian eddy statistics and diffusion in the mixed layer of the Southern Ocean. *J Mar Res* 66(4):441–463
98. McGillicuddy DJ, Robinson AR, Siegel DA, Jannasch HW, Johnson R, Dickey TD, McNeil J, Michaels AF, Knap AH (1998) Influence of mesoscale eddies on new production in the Sargasso Sea. *Nature* 419:263–266
99. Oschlies A, Garçon V (1998) Eddy-induced enhancement of primary production in a model of the North Atlantic Ocean. *Nature* 394:266–269
100. Karl DMEA (2003) Temporal studies of biogeochemical processes determined from ocean time-series observations during the JGOFS era. In: Fasham MJR (ed) Ocean biogeochemistry. Academic, New York, pp 239–267
101. Roussenov V, Williams RG, Mahaffey C, Wolff GA (2006) Does the transport of dissolved organic nutrients affect export production in the Atlantic Ocean? *Global Biogeochem Cycles* 20(3):GB3002
102. Mahaffey C, Williams RG, Wolff GA, Anderson WT (2004) Physical supply of nitrogen to phytoplankton in the Atlantic Ocean. *Global Biogeochem Cycles* 18, GB1034
103. Mather RL, Reynolds SE, Wolff GA, Williams RG, Torres-Valdes S, Woodward EMS, Landolfi A, Pan X, Sanders R, Achterberg EP (2008) Phosphorus cycling in the North and South Atlantic Ocean subtropical gyres. *Nat Geosci* 1(7):439–443
104. Torres-Valdés S, Roussenov VM, Sanders R, Reynolds S, Pan X, Mather R, Landolfi A, Wolff GA, Achterberg EP, Williams RG (2009) Distribution of dissolved organic nutrients and their effect on export production over the Atlantic Ocean. *Global Biogeochem Cycles* 23. doi:[10.1029/2008gb003389](https://doi.org/10.1029/2008gb003389)
105. Davis CS, McGillicuddy DJ Jr (2006) Transatlantic abundance of the N₂-fixing colonial cyanobacterium *Trichodesmium*. *Science* 312(5779):1517–1520. doi:[10.1126/science.1123570](https://doi.org/10.1126/science.1123570)

106. Mahaffey C, Michaels AF, Capone DG (2005) The conundrum of marine N₂ fixation. *Am J Sci* 305(6-8 SPEC. ISS.):546–595
107. Ferrari R, Nikurashin M (2010) Suppression of eddy diffusivity across jets in the Southern Ocean. *J Phys Oceanogr* 40(7):1501–1519. doi:[10.1175/2010JPO4278.1](https://doi.org/10.1175/2010JPO4278.1)
108. Hakkinen S, Rhines PB (2009) Shifting surface currents in the northern North Atlantic Ocean. *J Geophys Res C Oceans* 114(4):C04005
109. Hátún H, Sando AB, Drange H, Hansen B, Valdimarsson H (2005) Influence of the Atlantic subpolar gyre on the thermohaline circulation. *Science* 309(5742):1841–1844
110. Sarmiento JL, Slater R, Barber R, Bopp L, Doney SC, Hirst AC, Kleypas J, Matear R, Mikolajewicz U, Monfray P, Soldatov V, Spall SA, Stouffer R (2004) Response of ocean ecosystems to climate warming. *Global Biogeochem Cycles* 18(3)
111. Campbell JW (1995) The lognormal distribution as a model for bio-optical variability in the sea. *J Geophys Res Oceans* 100(C7):13237–13254. doi:[10.1029/95jc00458](https://doi.org/10.1029/95jc00458)
112. Palter JB, Lozier MS (2008) On the source of Gulf Stream nutrients. *J Geophys Res Oceans* 113(C6), C06018. doi:[10.1029/2007jc004611](https://doi.org/10.1029/2007jc004611)
113. Iudicone D, Speich S, Madec G, Blanke B (2008) The global conveyor belt from a Southern Ocean perspective. *J Phys Oceanogr* 38(7):1401–1425
114. Talley LD, Reid JL, Robbins PE (2003) Data-based meridional overturning streamfunctions for the global ocean. *J Climate* 16(19):3213–3226